PROPERTIES OF THIN YTTRIUM OXIDE DIELECTRIC FILMS

by

ERNEST B. RIEMANN

B. Eng. (Physics), McMaster University, 1969

A THESIS SUBMITTED IN PARTIAL FULFILMENT OF

THE REQUIREMENTS FOR THE DEGREE OF

MASTER OF APPLIED SCIENCE

in the Department of

Electrical Engineering

We accept this thesis as conforming to the

required standard

Research Supervisor.....

Members of the Committee.....

.....

Head of the Department.....

Members of the Department

of Electrical Engineering

THE UNIVERSITY OF BRITISH COLUMBIA

December, 1971

In presenting this thesis in partial fulfilment of the requirements for an advanced degree at the University of British Columbia, I agree that the Library shall make it freely available for reference and study. I further agree that permission for extensive copying of this thesis for scholarly purposes may be granted by the Head of my Department or by his representatives. It is understood that copying or publication of this thesis for financial gain shall not be allowed without my written permission.

Department of Electrical Engineering.

The University of British Columbia
Vancouver 8, Canada

Date Jan 3, 1972.

ABSTRACT

A study has been made of the properties of thin yttrium oxide dielectric films prepared by the electron beam evaporation of high purity Y_2O_3 powder.

Films deposited on freshly cleaved NaCl crystals and on polished n-type silicon were examined in the electron microscope. The specimens were found to be polycrystalline, with a crystal size of the order of 100 Å. The structure was found to be essentially the same as found for bulk Y_2O_3. D.C. conduction measurements were made on films of various thicknesses. The characteristics were found to be bulk-limited, with the conductivity decreasing at lower pressures. An activation energy of 0.6 eV was found. The conduction mechanism was believed to be Poole-Frenkel emission of electrons from donor centers into the Y_2O_3 conduction band. The donor centers were believed to be interstitial yttrium atoms rather than oxygen vacancies because of the pressure dependence observed in conductivity.

Step response measurements were made, and the results explained on the basis of a loss peak with a most probable relaxation time of 200 seconds. The relaxation of oxygen atoms dissolved in the anion defective Y_2O_3 lattice was assumed to be the mechanism. The results of step response and A.C. bridge loss measurements indicated that different relaxation mechanisms are dominant in different frequency ranges.

Internal photoemission measurements were made on Al-Y_2O_3-Al sandwiches. The energy barrier between the electrodes was found to be trapezoidal, with barrier heights of 3.14 and 3.72 eV.

TABLE OF CONTENTS

LIST OF ILLUSTRATIONS

ACKNOWLEDGEMENT

I wish to thank my research supervisor, Dr. L. Young, for his encouragement and guidance in the course of this investigation.

Grateful acknowledgement is given to the National Research Council for supporting this work with a Science Scholarship.

Thanks are also due to Mr. B. Wong for doing some of the D.C. conduction measurements, and Miss L. Morris for typing this thesis.

I. INTRODUCTION

High quality thin dielectric films are vital to the fabrication of many solid state devices. The films provide insulation, and are used for diffusion masking, surface passivation and hermetic sealing. To date, SiO_2, Si_3N_4, Al_2O_3, Ta_2O_5 and evaporated SiO have been the principal dielectrics used in electronic devices. It is desirable to find other dielectric materials that give better performance, higher reliability and lower cost.

A number of attributes are desirable in a dielectric used for device fabrication. Some of these are:

(1) Good insulating properties (low pinhole density, high breakdown field strength, high permittivity, low losses.)

(2) Low ionic mobility at adequate operating fields and temperatures.

(3) Low surface-state density when deposited on semiconductor material.

(4) Ease of production.

In this thesis, the properties of thin yttrium oxide dielectric films have been investigated. Previous work by Campbell[1] had shown these films to have low losses and interesting dielectric properties.

In the next chapter, the techniques used in sample preparation are discussed.

Chapter III is concerned with the study of thin yttrium oxide films by electron microscopy, in order to determine their physical structure.

Chapter IV deals with the D.C. conduction properties of these films, and how these properties may be understood by considering the structure of the Y_2O_3 crystal lattice.

In Chapter V, the results of step response and A.C. loss measurements are given.

Chapter VI deals with the energy barrier height determination at the Al-Y_2O_3 interface in Al-Y_2O_3-Al devices.

Finally, in Chapter VII the concluding remarks and recommendations for further research are given.

II. SAMPLE PREPARATION

The yttrium oxide films were evaporated in an electron beam apparatus with a 10-inch diffusion pump capable of reaching pressures as low as 10^{-6} torr without liquid nitrogen cooling. A Brad-Thomson type 776 W 9kW water-cooled electron gun provided the electron beam used for heating the compressed Y_2O_3 powder. It was possible to apply beam powers of up to 800 watts (for 20 kV accelerating voltage and 40 ma beam current) to an area as small as 25 mm.^{2}. The evaporation procedure was similar to that used by Campbell[1]. 99.99% purity yttrium oxide powder was packed firmly into a boron nitride crucible before insertion into the vacuum system. The material was outgassed for five minutes with a low power electron beam. When the vacuum reached 1×10^{-5} torr, oxygen was bled into the system and the pressure was held at 5×10^{-5} torr by throttling back the high vacuum valve. The film thickness was monitored during evaporation by depositing Y_2O_3 simultaneously on the substrate and a quartz crystal oscillating at a 5 MHz rate. The mass deposited on the crystal decreased the oscillating frequency, which was mixed with the output of a variable oscillator set near 5 MHz. The frequency difference was a linear function of film thickness, assuming constant film density. The constant of proportionality was found by measuring the thickness of a number of deposited films with a Talysurf*. The equation

$$d = 3.24\Delta f$$

where d = film thickness (Å) and $\Delta f \equiv$ change in frequency (Hz), was found to be accurate within 10% by comparison with Talysurf measurements.

Post-deposition thickness measurements were made by Talysurf or

---

* Made by Taylor Hobson Ltd.

Angstrometer.

The Talysurf is a mechanical device that measures the amplified mechanical movement of a stylus with respect to a reference plane.

The Angstrometer measures a fringe displacement caused by the interference of monochromatic light (Na yellow, 5890 Å) between the film to be measured and a Fizeau flat in contact with the film. A layer of highly reflecting aluminum was deposited on the insulating film to facilitate measurement. The thickness is given by

$$t = \frac{d}{D} \frac{\lambda}{2} \tag{1}$$

where $t \equiv$ film thickness

$D \equiv$ distance between fringes

$d \equiv$ fringe step

$\lambda = 5890$ Å

Both methods were considered to be accurate to about ± 100 Å.

After deposition the films were allowed to cool slowly in an oxygen ambient for fifteen minutes. The films were then baked in air for sixteen hours at 150°C. Some problems were encountered with the first films, which had many pinholes. The cause was found to be spattering of material from the crucible during evaporation. This was controlled by first fusing the surface of the Y_2O_3 powder and beginning the evaporation, then rotating the substrate into position over the cruicible.

Two types of substrates were used, Dow Corning 7059 aluminosilicate glass and silicon wafers. The former were cleaned with propyl alcohol, chromic acid and distilled water, then dried in air. A metal film typically 2000 Å thick was evaporated onto the substrate in an Edwards diffusion pump vacuum system. Aluminum, indium and gold were used. The 99.999% purity Al wire

was cleaned in KOH solution before placement on the tungsten heater wire. The aluminum was melted carefully and a small quantity was evaporated with the shutter in place between the heater and substrate. This allowed impurities to boil off. The shutter was opened for the evaporation, then shut again before all the aluminum had evaporated to minimize the evaporation of tungsten and other impurities from the heater wire. Evaporation rates as high as 1500 Å/min were found to give good films. The thickness was monitored with another quartz crystal oscillator.

Similar precautions were used in evaporating the other metals, except that propyl alcohol was used for cleaning.

Y_2O_3 films of varying thicknesses were then evaporated onto the metal films, using deposition rates in the 100 to 1000 Å per minute range. Higher rates were found to yield highly stressed films that cracked on cooling.

Metal counterelectrodes of various areas and thicknesses were then evaporated onto the oxide film. For internal photoemission studies, the counterelectrode films were made between 100 and 150 Å thick. For other measurements, more durable counterelectrodes of several thousand angstroms thickness were employed.

The structures discussed above are illustrated in Fig. 1.

The other substrates used were 0.3-0.6Ω-cm n-type polished silicon wafers one inch in diameter, purchased from the Monsanto Company. Yttrium oxide films were evaporated onto the silicon slices as before. A layer of antimony doped gold one to two thousand angstroms thick was evaporated onto the unpolished (reverse) side of the wafer. The antimony was driven into the silicon by diffusion at 400°C in a hydrogen atmosphere of 500 mm Hg pressure for five minutes. The resulting heavily doped n^+ region permitted ohmic contact to be made to the silicon.

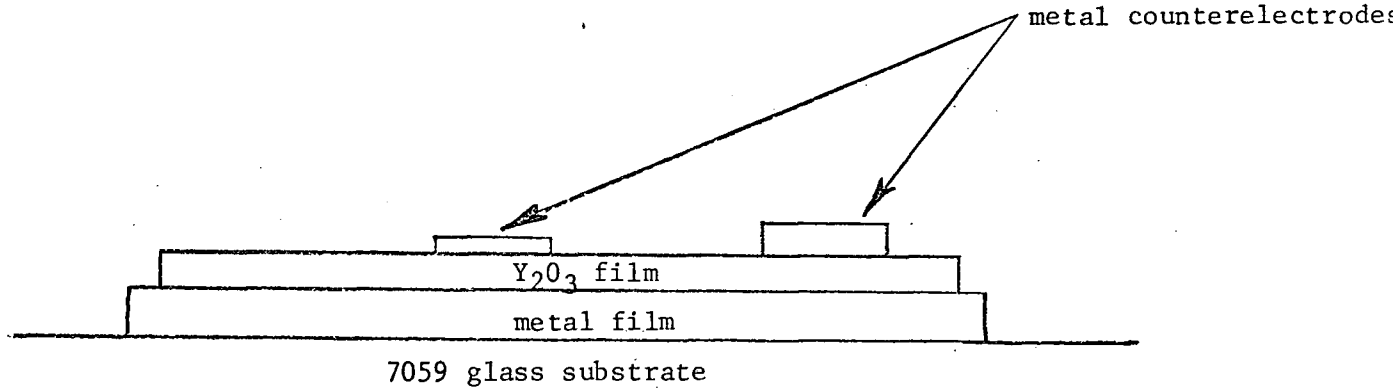

Fig. 1

MIM Structure

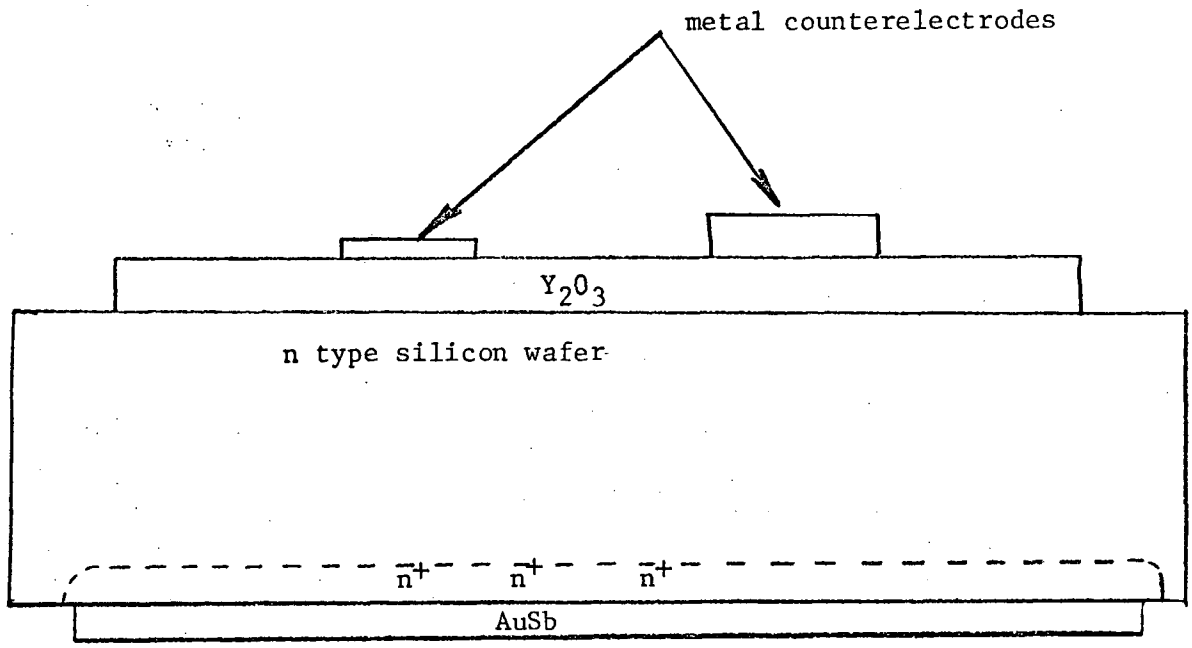

Fig. 2

MIS Structure

III. ELECTRON MICROSCOPY Of THIN Y_2O_3 FILMS

1. Introduction

A polycrystalline material yields a ring diffraction pattern for which it can be shown that

$$Dd = 2L\lambda, \quad \text{where} \tag{1}$$

$D \equiv$ diffraction ring diameter

$L\lambda \equiv$ camera constant

$d \equiv$ interplanar spacing in crystal lattice.

Bragg's law for diffraction is

$$n\lambda = 2d \sin\theta, \quad \text{where} \tag{2}$$

$n \equiv$ an integer ≥ 1

$\theta \equiv$ angle between the incident beam and the crystal plane.

In a cubic lattice, the interplanar spacing d corresponding to a set of Miller indices {hkl} is

$$d = a_o/\sqrt{h^2 + k^2 + l^2} \tag{3}$$

where a_o is the lattice constant.

Combining eq. (1) and (3) gives

$$(\frac{a_o}{2L\lambda})D = \sqrt{h^2 + k^2 + l^2}\ , \text{ which} \tag{4}$$

is a straight line of slope $a_o/2L\lambda$ when $\sqrt{h^2 + k^2 + l^2}$ is plotted against D.

Two techniques were used to obtain diffraction patterns: selected area diffraction and reflection electron diffraction.

The selected area method begins with an image of the film. The selected area aperture (located in the objective lens image plane) defines the area of the object that can be seen. In normal operation, the objective lens and intermediate lens image planes are conjugate foci, so that an

enlarged image of the film is produced. To obtain a diffraction pattern, the focal length of the intermediate lens is decreased until the objective back focal plane is conjugate to the intermediate lens image plane. A diffraction pattern then appears at the intermediate lens image plane. While the intermediate lens focal length is being decreased, the image of the object gradually shrinks to a point, and a diffraction pattern forms around it.

In the reflection diffraction technique, no image can form since only diffracted electrons can reach the image screen.

2. Procedure

Yttrium oxide films (~200 Å thick) were evaporated onto freshly cleaved NaCl crystals. After cooling, the films were floated off the water-soluble substrate in distilled water and picked up with copper electron microscope grids. The films were then examined by transmission electron microscopy and diffraction.

In order to check the influence of the substrate on crystal structure, a fairly thick (~2000 Å) film of yttrium oxide was evaporated on polished n-type silicon and the structure was examined by reflection electron diffraction.

3. Results

Fig. 3 shows the photograph of a diffraction pattern obtained with an accelerating voltage of 75kV, using the selected area diffraction technique. The film was found to be polycrystalline bordering on amorphous, with random crystal orientation and a crystal size of about 75 Å or more.[2]

It was found that individual crystals could not be resolved, probably

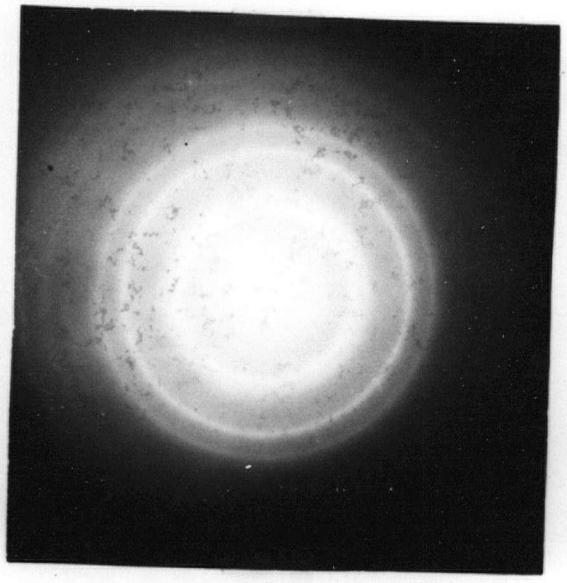

Fig. 3

Freshly deposited Y_2O_3 film.

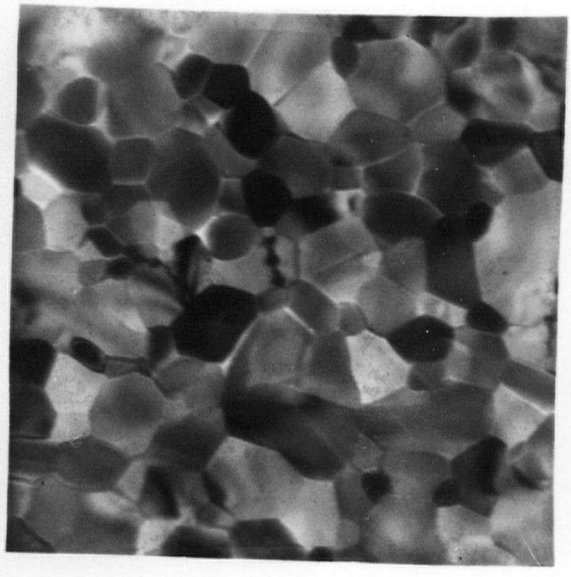

Fig. 4

Recrystallized Y_2O_3 film.

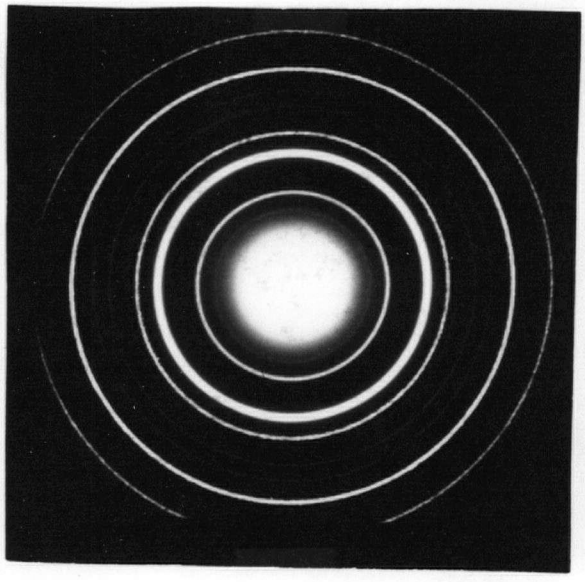

Fig. 5

Diffraction Structure of
Recrystallized film

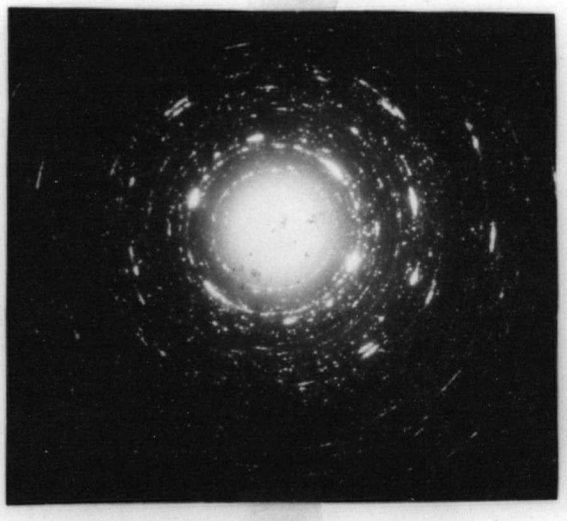

Fig. 6

Diffraction Pattern after

further recrystallization

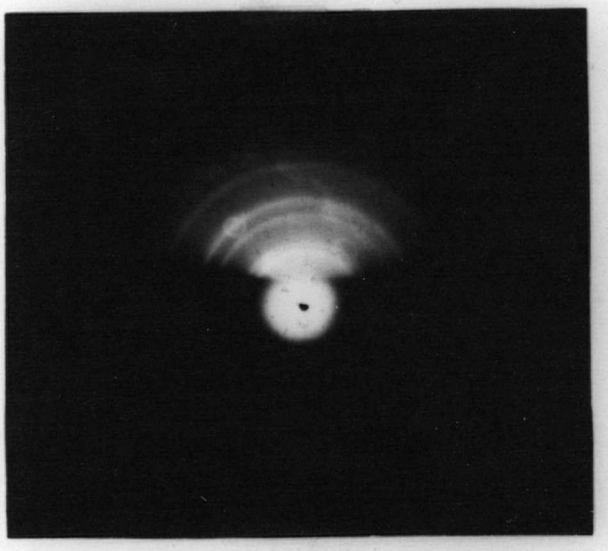

Fig. 7

Reflection electron diffraction

from Y_2O_3 on n-type polished silicon

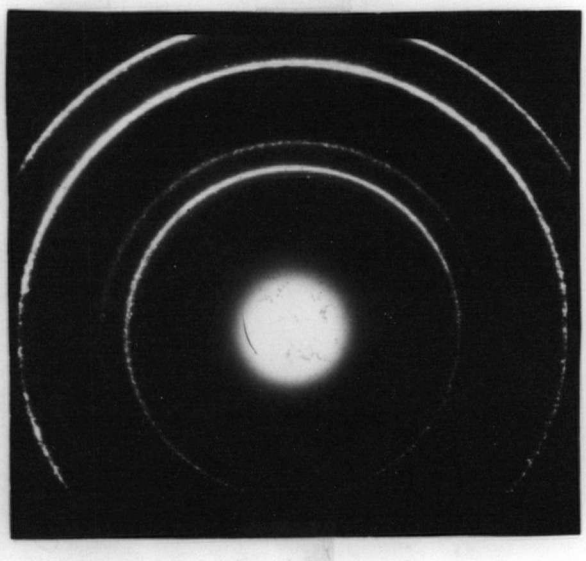

Fig. 8

Diffraction pattern

of gold film

because of diffraction by crystals of several orientations stacked vertically in the film.

When the films were heated with an intense electron beam, they were observed to recrystalize. An attempt was made to find the recrystallization temperature with a heating stage, but nothing was observed below 800°C, the thermal limit of the stage. Fig. 4 shows the structure of a recrystallized film at a magnification of X46,000. A diffraction pattern for this film is shown in Fig. 5. The pattern was observed to be more distinct, probably because of reduced random scattering of electrons from near-amorphous regions. The strong lines have diameters in the same ratios as in Fig. 3, but more rings can be resolved. This pattern was photographed using 100kV as the accelerating potential, resulting in larger diameter rings (due to the shorter electron wavelength.) than Fig. 3.

After further recrystallization by the beam, the pattern of Fig. 6 was obtained. The continuous diffraction rings of Fig. 5 are broken into rings of diffraction spots because of the smaller number of crystals in the path of the beam.

Fig. 7 shows a reflection electron diffraction pattern for yttrium oxide deposited on polished n-type silicon. The ring diameters again are in the same ratios as the brightest rings in Fig. 5, but the size of the overall pattern is reduced because of the proximity of the specimen and the photographic plate in the reflection method.

Finally, Fig. 8 shows the transmission diffraction pattern for a thin gold film that was used to determine the camera constant of the electron microscope for the particular control settings used. The value of the camera constant varies with the lens settings, and so the same settings must

be used in the specimen diffraction as for the calibration diffraction. The accuracy of the final results depends on the accuracy with which the camera constant is determined. A gold film was used because the crystal structure of gold and its lattice constant are well known.

4. Analysis

The camera constant of the electron microscope was determined with equation (4) to be

$$L\lambda = 5.82 \pm 0.02,$$

using the value of 4.087 Å for the lattice constant of gold.[3]

Table 1 shows an analysis of the diffraction pattern of yttrium oxide based on Fig. 5. The ring diameter ratios were found to be consistent with a simple cubic structure. The ring intensities were compared to existing data for polycrystalline Y_2O_3 powder and were found to be in excellent agreement. A few faint rings (consistent with the crystal structure) were observed in the electron diffraction but not in the X-ray pattern.

Fig. 9 shows a plot of $\sqrt{h^2 + k^2 + l^2}$ vs. ring diameter. The result is a straight line passing through the origin, indicating a good fit of the data to the simple cubic structure. From Fig. 9, the lattice constant was determined to be

$$a_o = 10.58 \pm 0.05 \text{ Å},$$

which is in excellent agreement with the value 10.605 ± 0.001 obtained by X-ray diffraction.[4]

The first four rings of Fig. 3 and Fig. 7 are analyzed in Tables 2 and 3. The ring diameters were found to be in the same ratios and have the same relative intensities as the bright Y_2O_3 diffraction rings of Fig. 5, within experimental error.

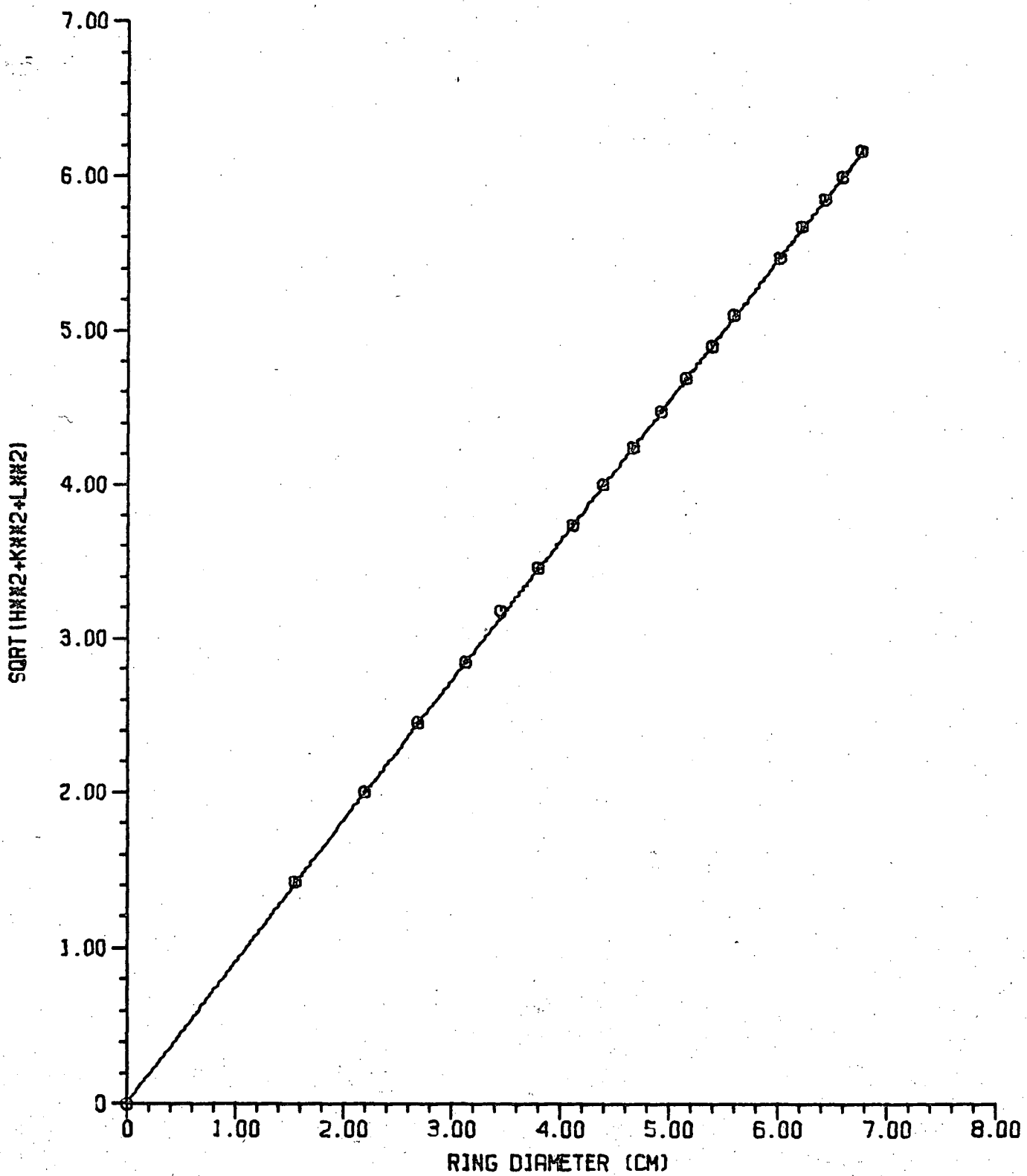

Fig. 9

$\sqrt{h^2+k^2+\ell^2}$ vs. D(cm) for Y_2O_3 Films

TABLE 1

ELECTRON DIFFRACTION RESULTS

Ring Diameter D (cm)	Ratio $R=\frac{D}{1.10}$	R^2	$h^2+k^2+l^2$	hkl	Intensity*	X-Ray Intensity(5)
1.55	1.41	1.99	2	110	f	-
2.20	2.00	4.00	4	200	m	-
2.69	2.45	6.00	6	211	b	14
3.12	2.84	8.08	8	220	vf	-
3.48	3.16	9.96	10	310	vf	-
3.80	3.46	12.0	12	222	vbll	100
4.12	3.74	14.0	14	321	f	-
4.40	4.00	16.00	16	400	vb	31
4.66	4.24	18.0	18	411	m	7
4.93	4.48	20.2	20	420	f	2
5.17	4.70	22.1	22	332	m	9
5.40	4.91	24.1	24	422	f	2
5.60	5.10	26.0	26	431 510	b	14
6.02	5.47	29.8	30	521	m	5
6.24	5.66	32.0	32	440	vb	61
6.43	5.84	34.1	34	530 433	f	3
6.60	6.00	36.0	36	600 442	vf	2

TABLE 1 (Continued)

D(cm)	R	R^2	$h^2+k^2+l^2$	hkl	I	X-Ray I
6.78	6.17	38.0	38	611 532	m	8
6.95	6.33	40.1	40	620	vf	2
7.13	6.48	42.1	42	541	m	8
7.30	6.64	44.1	44	622	b	43
7.46	6.78	46.0	46	631	m	11
7.62	6.93	48.0	48	444	m	10
7.78	7.08	50.1	50	550 710 543	f	4
7.93	7.22	52.0	52	640	vf	3
8.08	7.36	54.2	54	633 552 721	m	6
8.23	7.46	55.8	56	642	f	4

* vf very faint

f faint

m medium

b bright

vb very bright

TABLE 2

Y_2O_3 on NaCl, Unrecrystallized

D (cm)	$R=\frac{D}{0.707}$	R^2	$h^2+k^2+\ell^2$	Plane	Intensity
2.46	3.46	12	12	222	vb
2.84	4.03	16.2	16	400	vb
4.02	5.64	31.7	32	440	b
4.73	6.67	44.4	44	622	vb

±0.05

TABLE 3

Y_2O_3 On Silicon

D (cm)	$R=\frac{D}{0.468}$	R^2	$h^2+k^2+\ell^2$	Plane	Intensity
1.62	3.46	12.0	12	222	vb
1.90	3.96	15.7	16	400	b
2.66	5.66	32.0	32	440	b
3.12	6.65	44.2	44	622	m

±0.05

5. Discussion

Freshly prepared yttrium oxide films on sodium chloride and silicon were found to have the same structure. The films were polycrystalline, with a crystal size of the order of 100 A^{o}. Thus, it can be concluded that the crystal structure of the substrate material has little effect on the structure of the yttrium oxide films.

The films were found to have a simple cubic structure with a lattice constant of 10.58 ± 0.05 $\mathring{A}$, which is in good agreement with the existing data for bulk Y_2O_3.

Thus, it is evident that the metastable reduced oxide YO is present in only small quantities or not at all in the films.

The results found are in essential agreement with those of Hass, Ramsey and Thun[5], who examined the structure of La_2O_3 in the course of their work on optical coatings. However, their films were somewhat more amorphous than those studied here, possibly because they did not evaporate in an oxygen ambient. Also, they evaporated from tungsten boats, a lower temperature process than electron gun evaporation. As a result, their structure determination of La_2O_3 showed a hexagonal lattice with a c/a ratio of 1.63 instead of the value of 1.56 accepted for the bulk material. No such distortions of the crystal lattice were observed in this work.

The unit cell of the Y_2O_3 structure contains 32 yttrium and 48 oxygen ions[6]. The structure consists of subunits containing one cation centered within a cube of eight anion sites, of which only six are occupied. Half the cations are in subunits which have the unoccupied anion sites on the face diagonal, the other half have unoccupied sites on a body diagonal. The

subunits fit together so that the unoccupied anion sites form nonintersecting strings along the <111> directions of the crystal. These strings provide pathways along which the diffusion of oxygen ions would meet with relatively little resistance. Fully one-fourth of the anion sites in the sublattice are unoccupied, so that a high solubility of O_2 in Y_2O_3 would be expected.

IV. CONDUCTION IN THIN Y_2O_3 FILMS

1. Introduction

In thin insulating films, a variety of mechanisms can be responsible for carrier transport. For wide bandgap materials ($E_g > 3eV$), conduction is often due to the trapping and detrapping of carriers. This is particularly true for films more than a few hundred angstroms thick.

Semiconductor theory gives the following expression for the electron current density in an intrinsic insulator:

$$J = \sigma E = ne\mu E = e\mu\sqrt{N_c N_v}\, E \exp(-Eg/2kT) \qquad (1)$$

where $E \equiv$ electric field

$J \equiv$ current density

$\sigma \equiv$ conductivity

$n \equiv$ carrier concentration

$\mu \equiv$ carrier mobility

$E_g = 2(E_F - E_c) \equiv$ bandgap

$N_c, N_v \equiv$ insulator effective density of states in conduction and valence bands

$T \equiv$ absolute temperature

For favourable room-temperature values of $\sqrt{N_v N_c} = 3 \times 10^{19}$ cm^{-3}, $E_g = 3eV$, $\mu = 100$ cm^2/V sec, and $E = 10^6$ V/cm, the current density is only about 10^{-18} A/cm^2 (7), which is much less than the magnitude of the currents normally observed in thin film insulators. Furthermore, the observed activation energies for conduction are usually much smaller than $E_g/2$, so that intrinsic conduction cannot be the transport mechanism.

The conductivity of vacuum deposited thin films can be attributed to the unique nature of such films. Compounds are difficult to evaporate stoichiometrically because of the differing evaporation rates of the consti-

tuent atoms. Often, in the case of oxides, the films are reduced somewhat. During the evaporation of Y_2O_3, films deposited rapidly showed a brown discoloration that researchers on bulk Y_2O_3 have attributed to color centers associated with oxygen vacancies and trapped electrons[8]. Contamination with crucible material could also be a source of film defects. Evaporation of the crucible material many orders of magnitude slower than the evaporant can produce significant defect densities in dielectric films, since these materials have such a small intrinsic carrier concentration. Finally, the amorphous or near-amorphous nature of thin evaporated insulating films makes it likely that a high trap density will exist. In vacuum evaporated CdS, trapping densities as high as $10^{21}/cm^3$ have been reported[9].

Thus, it is likely that evaporated insulating films will have a high density of traps and acceptor or donor centers, and hence the conduction properties of these films must be studied with this defect structure in mind.

A number of conduction mechanisms have been proposed for insulating films between metal counterelectrodes.

The tunnel effect (from metal to metal) is a possible mechanism only for insulators less than 100 Å thick, and will not be considered here.

The Schottky effect is field enhanced thermionic emission over the barrier at a metal-insulator interface. If the barrier at the interface is assumed to be Coulombic, then the image force barrier lowering for an electron has been shown to be

$$\beta_s = \sqrt{\frac{e^3}{4\pi\varepsilon}} \tag{2}$$

and the conduction characteristic is

$$J = AT^2 \exp\{\frac{e\phi_B - \beta_s\sqrt{E}}{kT}\} \tag{3}$$

where $A \equiv$ constant

$\phi_B \equiv$ barrier height

It is unlikely that this mechanism can account for conduction in films with a high defect density, unless the films are quite thin, since trapping and space charge effects would be expected to dominate the conduction process in thick films.

The Poole-Frenkel effect, or field-assisted thermal emission of carriers over the Coulombic barrier of a donor center, was first applied by Frenkel to semiconductors[10].

In Fig. 1, the potential well associated with a trap of depth E_t is illustrated.

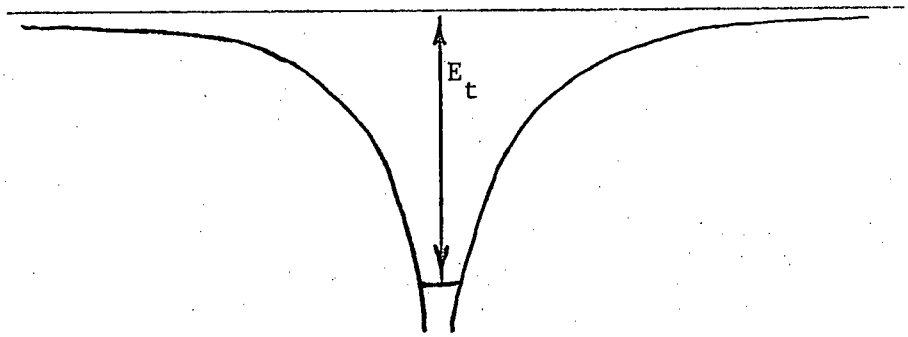

Fig. 1

The next diagram shows how the potential is modified by the presence of a uniform electric field E. The barrier is lowered in energy by $\Delta\phi$, which can be determined by finding the distance from the center of the potential distribution to the maximum in the energy function.

The Coulomb barrier has the potential

$$E_n = -\frac{e^2}{4\pi\epsilon x}$$

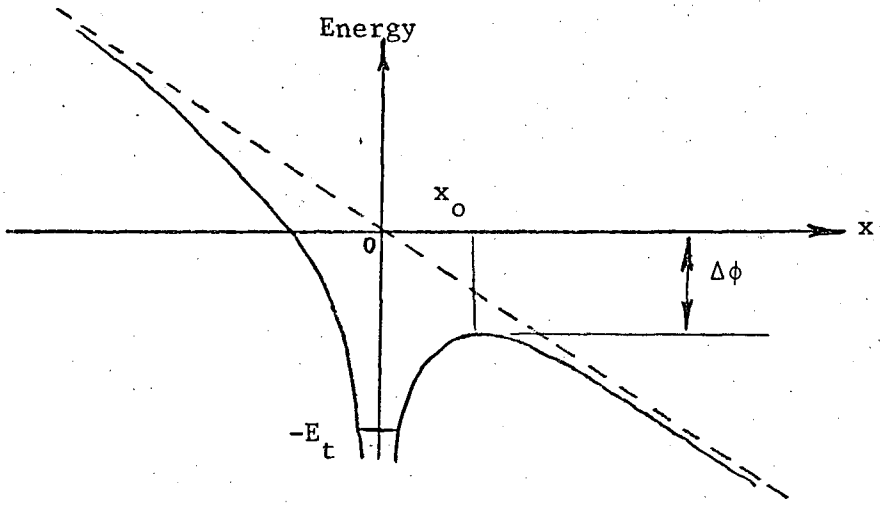

Fig. 2

In the presence of the field E, this becomes

$$E_n = \frac{-e^2}{4\pi\epsilon x} - eEx \tag{4}$$

The dielectric constant ϵ is the high frequency value, since the electron motion is too rapid for the lattice ions to follow. At x_o, $\frac{dE_n}{dx} = 0$, so $\frac{e^2}{4\pi\epsilon x_o^2} - eE = 0$, or

$$x_o = \frac{e}{\sqrt{4\pi\epsilon E}} \tag{5}$$

Thus, $\Delta\phi$ is

$$\Delta\phi = \sqrt{\frac{e^3E}{\pi\epsilon}} = \beta_{PF}\sqrt{E} \tag{6}$$

Frenkel assumed (as discussed later in this chapter) that the ionization potential E_g of the solid was reduced by the amount $\Delta\phi$, yielding the conduction law

$$\begin{aligned} J_F &= ne\mu E = e\mu N_c E \exp-\{[(E_g-\beta_{PF}\sqrt{E})]/2kT\} \\ &= J_o \exp\left(\frac{\beta_{PF}\sqrt{E}}{2kT}\right). \end{aligned} \tag{7}$$

Mead (1962)[11], in his work on Ta_2O_5 thin films, used the equation

$$J = G_o E \exp\{[(\beta_{PF}\sqrt{E}-V)]/kT\} \tag{8}$$

to explain his results. He assumed the conduction mechanism to be field-enhanced thermal emission from traps of depth V in the insulator forbidden bandgap. He derived (8) by assuming that the exponential dependence of J on E was similar to that of the Schottky effect, except that the barrier lowering was twice as large (as can be seen by comparing (2) and (6)). His equation is similar to Frenkel's, except that the coefficient of $\sqrt{E}$ is β_{PF}/ kT^*. Mead's data gave a fit of 21 and 27 for the dielectric constant. These values are too large for the high-frequency dielectric constant of Ta_2O_5.

Other workers who used (8) to explain their results have typically found that values of ε about four times too large were necessary to fit their data. Hartman[12] et al concluded that (8) did not adequately fit the data on Ta_2O_5 and SiO films because of the difficulty with the permittivity. Although the Schottky conduction equation gave a much better fit for ε, it could not explain the variation of current with film thickness that was observed.

Simmons[13] has suggested a theory of Poole-Frenkel emission to resolve the difficulty. In this theory, Simmons considered an insulator model with deep donor centers and shallow neutral traps, as illustrated below.

If we assume that the number of electrons in the conduction band is negligibly small compared to the number of trapped electrons, then we can equate the number of electrons missing from donor centers to the number of

---

*If eq. (8) is correct, it would be possible to differentiate between Schottky emission (eq. (3)) and Poole-Frenkel emission by the difference in slope of the log T vs. $\sqrt{E}$ plots. The Poole-Frenkel slope would be twice the Schottky slope.

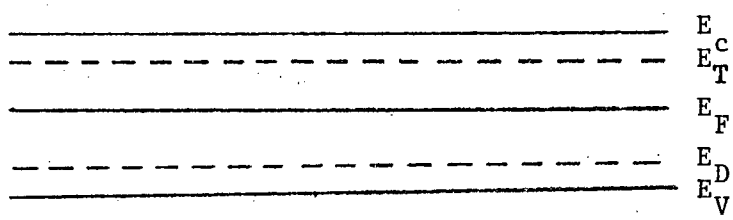

Fig. 3

occupied traps, for $E_F - E_D >> kT$ and $E_T - E_F >> kT$:

$$N_D \exp\{-(E_F - E_D)/kT\} = N_T \exp\{-(E_T - E_F)/kT\} \tag{9}$$

where $N_D \equiv$ effective donor density of states

$N_T \equiv$ effective trap density of states.

Solution of (9) for the Fermi energy gives

$$E_F = \frac{1}{2}(E_D + E_T) + \frac{1}{2} kT \ln(N_D/N_T) \tag{10}$$

Thus, at zero field, the number of free electrons is

$$\begin{aligned} n &= N_c \exp-\{[E_c - E_F]/kT\} \\ &= N_c \sqrt{N_D/N_T} \exp-\{[2E_c - (E_T + E_D)]/2kT\} \end{aligned} \tag{11}$$

and the zero field conductivity is $\sigma_o = ne\mu$

$$= e\mu N_c \sqrt{N_D/N_T} \exp\{[2E_c - (E_T + E_D)]/2kT\} \tag{12}$$

When an electric field is applied, the donor energy barrier $E_c - E_D$ is lowered by the Poole-Frenkel value. Because the traps are assumed to be neutral, their energy barrier is not affected, so that the number of free electrons in the conduction band is

$$n = N_c \sqrt{N_D/N_T} \exp\{[(E_c - E_T) + (E_c - E_D) - \beta_{PF}\sqrt{E})]/2kT\} \tag{13}$$

Hence,

$$\sigma = \sigma_o \exp(\beta_{PF}\sqrt{E}/2kT). \tag{14}$$

We see that the conductivity varies with the field in a manner normally associated with the Schottky effect at a neutral barrier. The current is

$$J = \sigma E = \sigma_o E \exp\{\beta_{PF}\sqrt{E}/2kT\} \qquad (15)$$

Stuart[14] and Hill et al[15] have explained their conduction data on SiO with equation (15). The fit for ε was found to be good in the high-field region of conductivity.

There are several difficulties with Simmons' theory.

First, the calculation of the electron concentration using the Fermi level requires that the insulator be in equilibrium. Poole-Frenkel emission, however, is a non-equilibrium effect, and so the methods used to derive (15) are somewhat contradictory.

It is also unrealistic to assume that the trap energy barrier will remain unaffected by the presence of an electric field.

The barrier height for emission from traps is smaller than that for emission from donors in Simmons' model, and the trap barrier lowering should give the largest contribution to the conduction current.

The major difficulty with equation (12) concerns the activation energy of the conduction process. In commonly used insulators such as SiO_2, SiO and Al_2O_3, as well as Y_2O_3, the energy difference between the Fermi level and the insulator conduction band is 3eV or more (the bandgap is 6-8eV). The Poole-Frenkel barrier lowering for $E = 10^6$V/cm (near breakdown), and $\varepsilon_r = 3$ is only 0.44 eV. This amount of barrier lowering is not nearly large enough to allow a significant number of donors below the Fermi energy to be ionized at room temperature. The activation energies usually observed for Poole-Frenkel currents are about 0.5 eV. Stuart found 0.4 eV fitted the results for SiO, and 0.6 eV was found for Y_2O_3 films.

Thus, Simmons' theory suggests higher activation energies than are found in practise.

An equation that gives better results can be found by considering the methods of Frenkel's original paper. Consider an insulator with shallow donors that are normally filled with electrons at room temperature. If N_D is the total number of donors and n_D the number of occupied donors we can define an occupancy factor by

$$f = \frac{n_D}{N_D} \tag{16}$$

The rate of release of electrons from donors in the presence of a field (assuming Poole-Frenkel barrier lowering) will be

$$R = f\, N_D\, \nu \exp-\{[(E_c-E_D)-\beta_{PF}\sqrt{E}]/kT\} \tag{17}$$

where $\nu \equiv$ vibration frequency of trapped electrons.

The rate of capture of electrons will be

$$c = (1 - f)N_D\, Js/e, \text{ where} \tag{18}$$

$J \equiv$ current density

$s \equiv$ capture cross-section of empty donors. For shallow donors, we would expect the occupancy factor f to be field-dependent.

In equilibrium, the rates of electron capture and release are equal, so that

$$\frac{1-f}{f} = e\nu \exp-\{[(E_c-E_D) - \beta_{PF}\sqrt{E}]\}/Js \tag{19}$$

If we assume that the number of electrons released from donors by the field is small, then $f \sim 1$, and the current is given by

$$J = ne\mu E = (1-f)N_D e\mu E$$

$$= \frac{N_D e^2 \mu E \nu}{Js} \exp-\{[(E_c-E_D)-\beta_{PF}\sqrt{E}]/kT\} \tag{20}$$

Solving for the current gives

$$J = e\sqrt{\frac{N_D \mu \nu\, E}{s}} \exp-\{[(E_c-E_D)-\beta_{PF}\sqrt{E}]/2kT\} \tag{21}$$

This equation is similar to Simmons', and it gives the same slope on a log J vs. $\sqrt{E}$ plot as the Schottky conduction law. The pre-exponential variation with the field is $\sqrt{E}$ rather than E. This is unimportant at high fields, where the exponential term dominates.

2. Experimental Procedures

The D.C. conduction characteristics were measured with a Keithley 417 high-speed picoammeter in series with a variable voltage supply. Shielded cables were used to minimize transients. For the high temperature measurements, the sample was placed in a Statham SD6 oven. An iron-constantan thermocouple was installed near the sample and was used to measure the temperature.

The conduction characteristics were found to drift over a period of time, probably because of step response effects in the dielectric material. It was found necessary to wait for anywhere between a few minutes to an hour (depending on the applied voltage) for the conduction to approach its limiting value to within a few percent. Space charge effects or ionic currents are also a possible explanation of the observed drift.

3. Experimental Results

The thin Y_2O_3 films were found to have bulk-limited conduction characteristics roughly similar to those found for SiO films by Stuart. In Fig. 4, log I is plotted against $\sqrt{V}$ for three different thicknesses of film. The plots are linear in the high-field region where the voltage is greater than about 15 volts. The films had aluminum counterelectrodes.

In Fig. 5, the variation of the conduction characteristics with temperature is plotted. Higher currents were observed at higher temperatures.

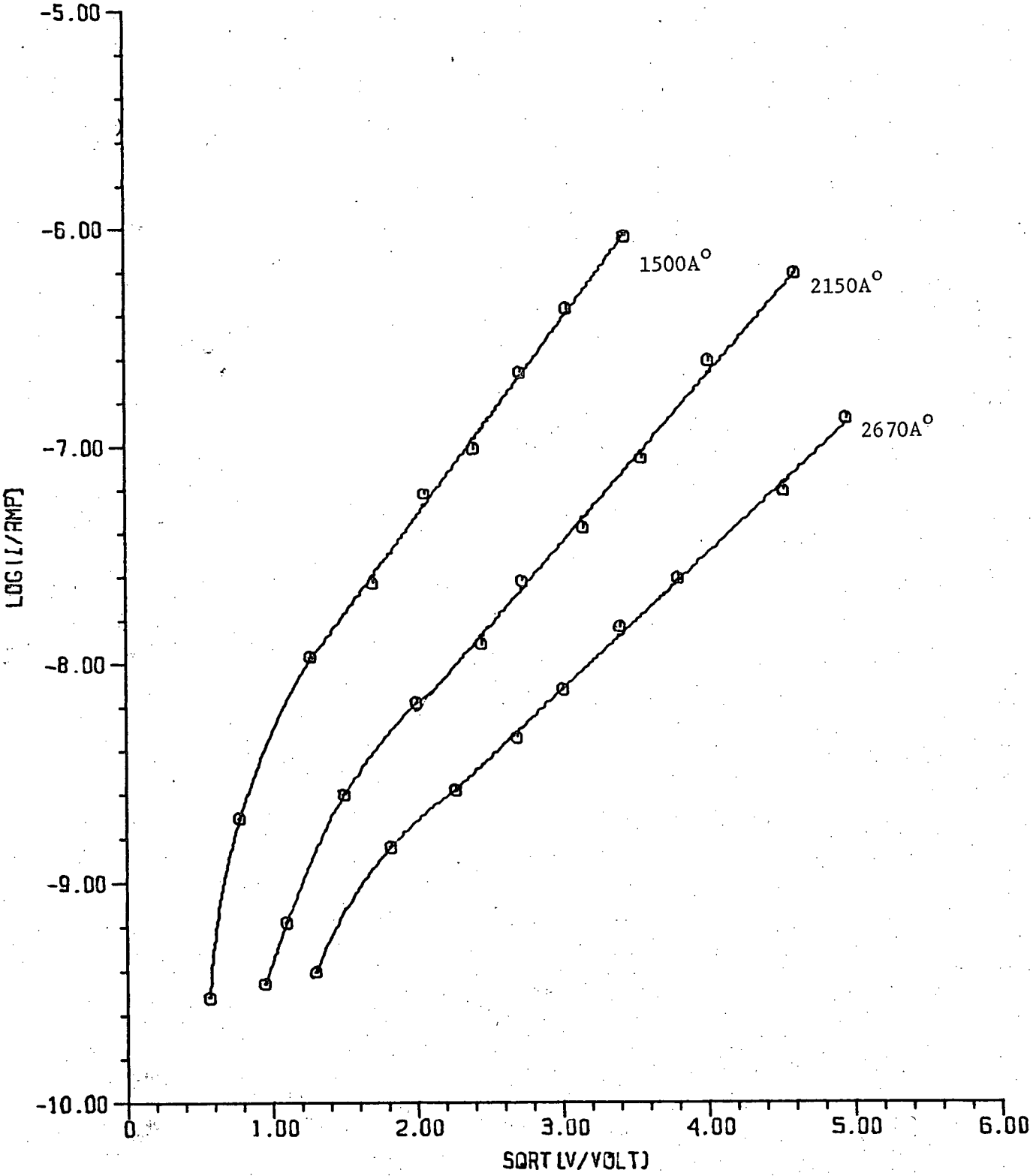

Fig. 4

Log I vs. $\sqrt{V}$

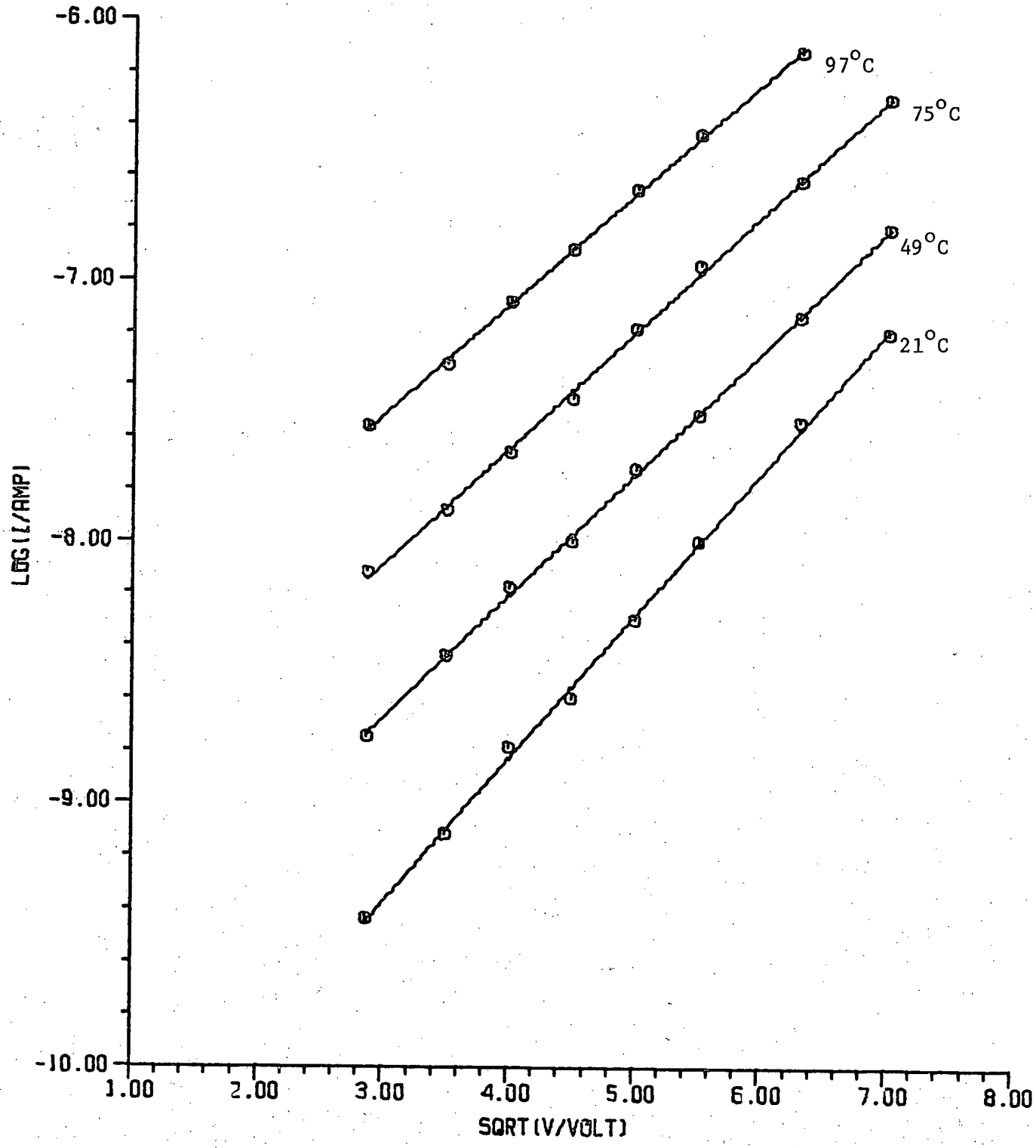

Fig. 5

Log I vs. $V^{1/2}$ for Different Temperatures (d = 4680A°.)

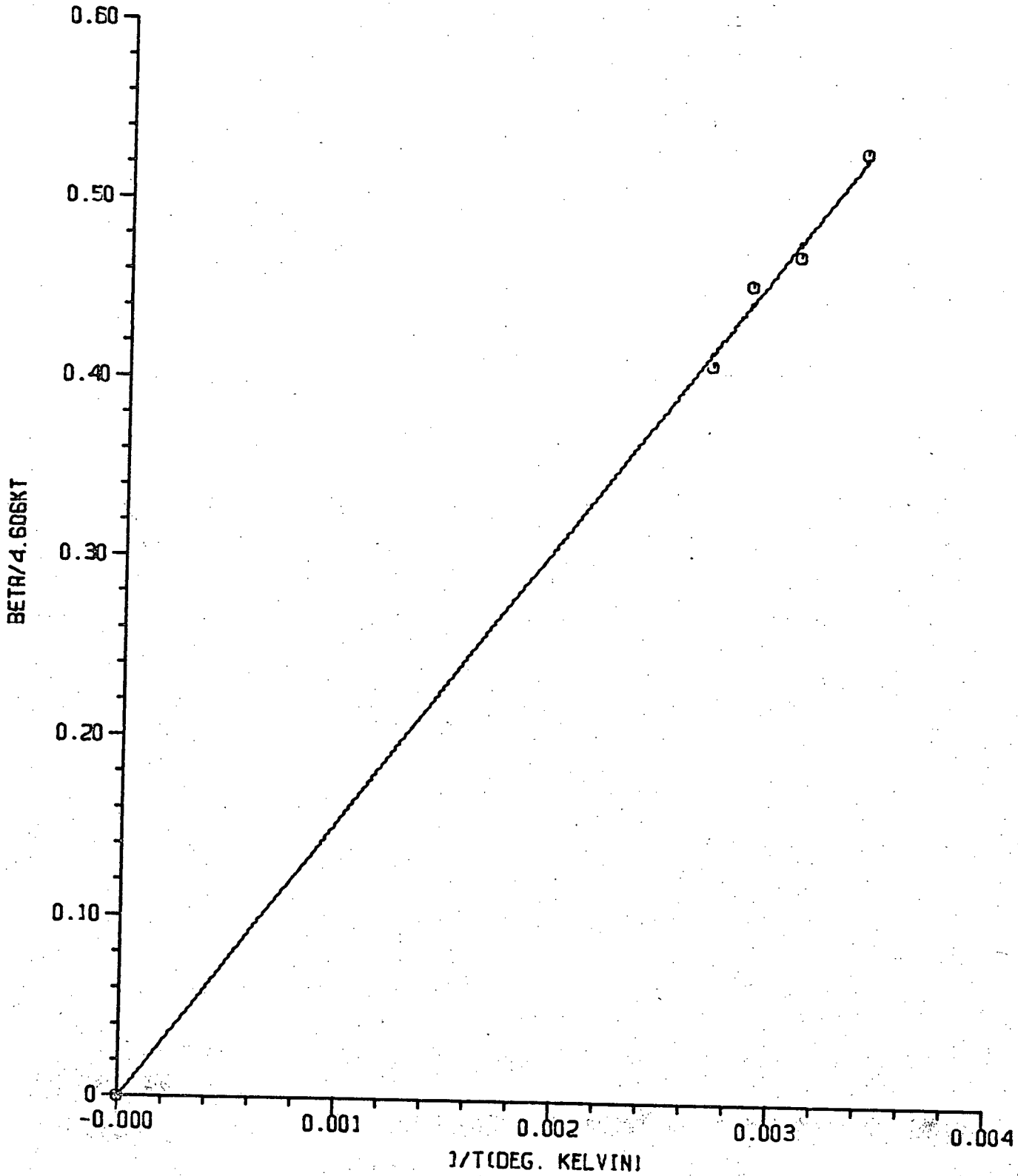
0.60
0.50
0.40
0.30
0.20
0.10
0
BETA/4.606KT
-0.000
0.001
0.002
0.003
0.004
1/T(DEG. KELVIN)

Fig. 6

Fig. 6 shows a plot of $(\frac{\beta}{2})/(2.303\ kT)$ vs. $\frac{1}{T}$ derived from Fig. 5. A fit for β in the equation

$$I = I_o \exp-\{\frac{w-\beta\sqrt{V}}{2kT}\} \tag{22}$$

was made with Fig. 6, and the relative permittivity of the film was found using

$$\beta = \sqrt{\frac{e^3}{\pi\epsilon d}} \tag{23}$$

The film thickness was measured to be 4680 ± 200 Å on the Sloan M100 Angstrometer. The dielectric constant was found to be

$$\epsilon_r = 3.2 \pm 0.2 \tag{24}$$

The refractive index of a Y_2O_3 film on silicon was determined by ellipsometry[16] at a wavelength of 6328 A° to be

$$n = 1.75 \pm 0.01 \tag{25}$$

This result was found by solving the ellipsometry equation on the U.B.C. IBM 360 computer with iterative methods.

This gives the permittivity

$$\epsilon_r = n^2 = 3.05,$$

which is in good agreement with the value of the permittivity found from the conduction measurements. The effect of polarity reversal on the conduction measurements is illustrated in Fig. 7 for a film with gold and indium counterelectrodes. These metals were selected because of their large work function difference. The forward and reverse conduction characteristics were found to be virtually identical. Thus, the conductivity of Y_2O_3 is bulk-limited rather than emission limited. The very slight asymmetry in conductivity observed is probably due to an internal field in the oxide, as would be expected for contacts with different work functions.

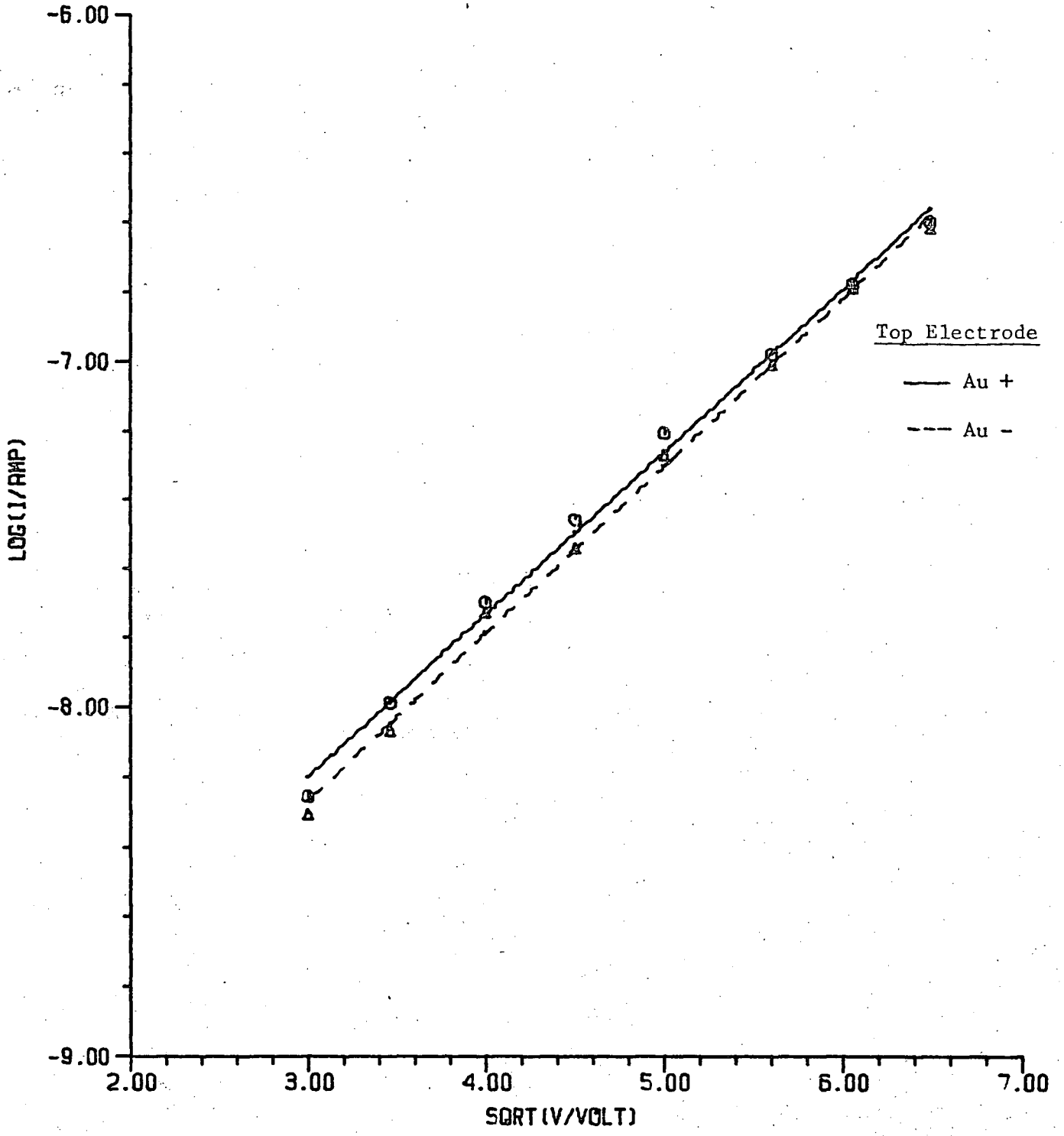

Fig. 7

Effect of Polarity Reversal on D.C. Conduction

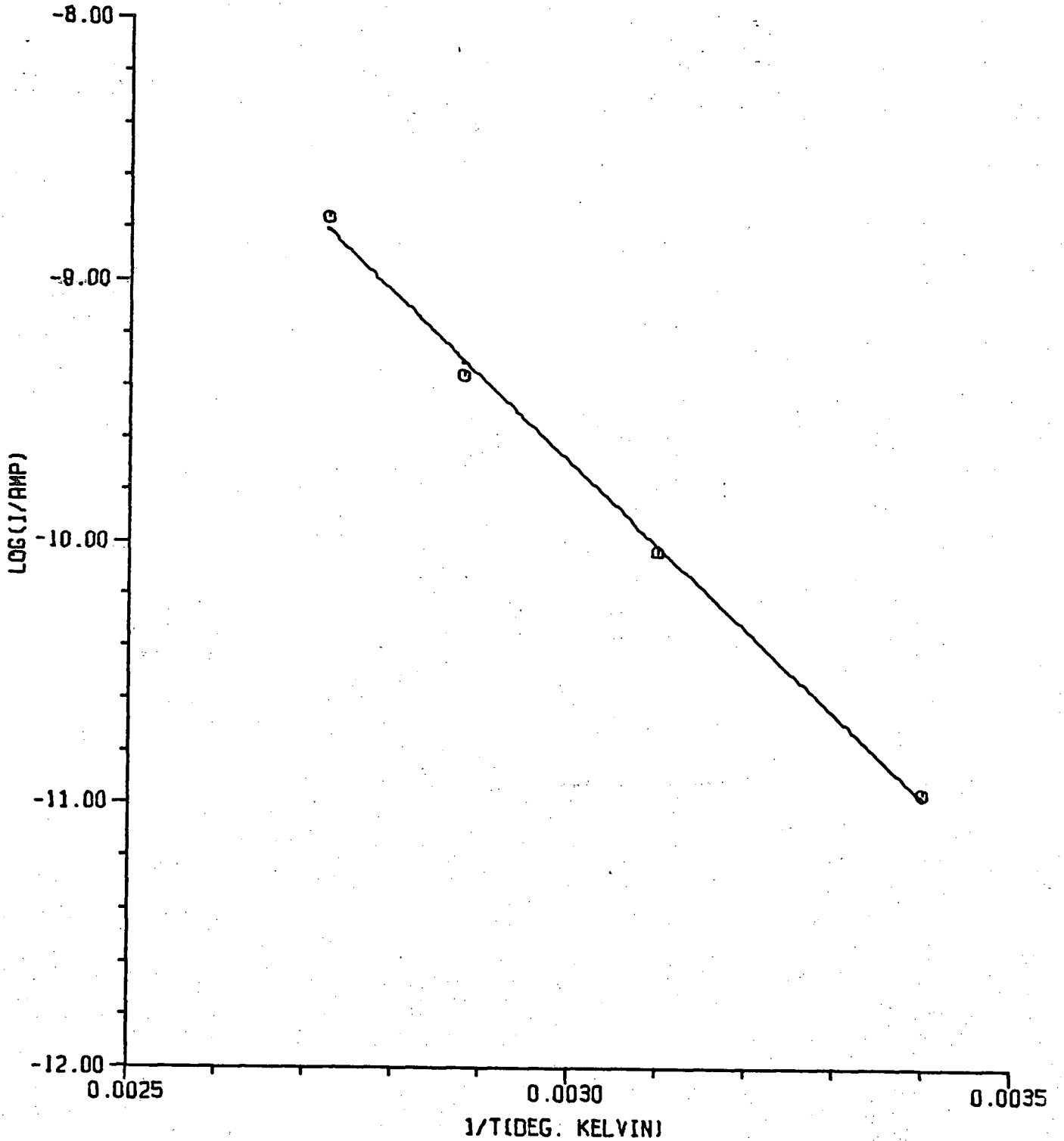

Fig. 8

Determination of Activation Energy

The activation energy of the conduction process was found to be independent of temperature, as can be seen from the straight line plot of log I vs. $\frac{1}{T}$ shown in Fig. 8. The activation energy was found to be 0.58 $\pm$ 0.05eV.

The low pressure D.C. conduction characteristics are plotted for different temperatures in Fig. 9. The pressure was about 50 μ Hg. The film thickness was measured to be 3240 $\pm$ 100 $\mathring{A}$ with a Talysurf.

The current was observed to decrease by several orders of magnitude over a period of a few hours after the pressure was reduced. Fig. 10 shows a plot of $(\beta/2)/(2.303kT)$ based on the slopes of Fig. 9. The value of the relative permittivity that was found to fit the conduction characteristics was $\epsilon = 11.2 \pm 0.7$, or roughly four times the high-pressure value. The activation energy was found from Fig. 11 to be 0.63 $\pm$ 0.05eV, almost the same as the high-pressure value.

Fig. 12 gives the D.C. conduction of three different counterelectrodes on the same Y_2O_3 film. The reproducibility is seen to be fairly good. The variation observed can be attributed to thickness variations in the thin film.

4. Discussion

The conduction characteristics of thin Y_2O_3 films were found to fit equation (21) quite well. The non-linearity observed at low fields is similar to that reported by Hartman et al[6] (1966) and Stuart[8] (1967) for SiO films. The conductivity in this region is believed to be partly bulk-limited and partly ohmic. This view is supported by the fact that the current for all three thicknesses begins to approach the same limiting value at low applied voltages. In the high-field region where $E_{applied} \gtrsim 10^5$ volts/cm, the

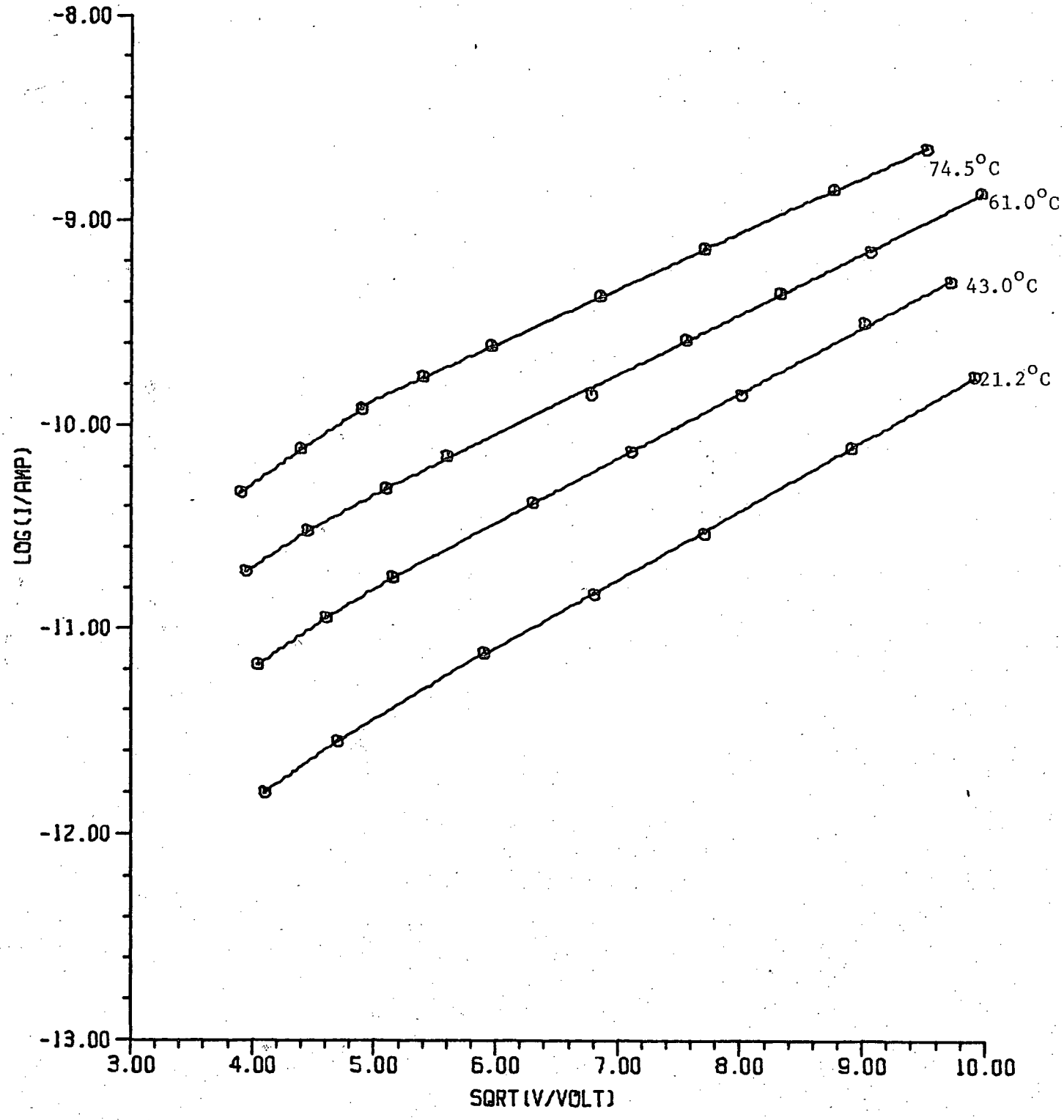

Fig. 9

D.C. Conduction at Low Pressure (P=50μ)

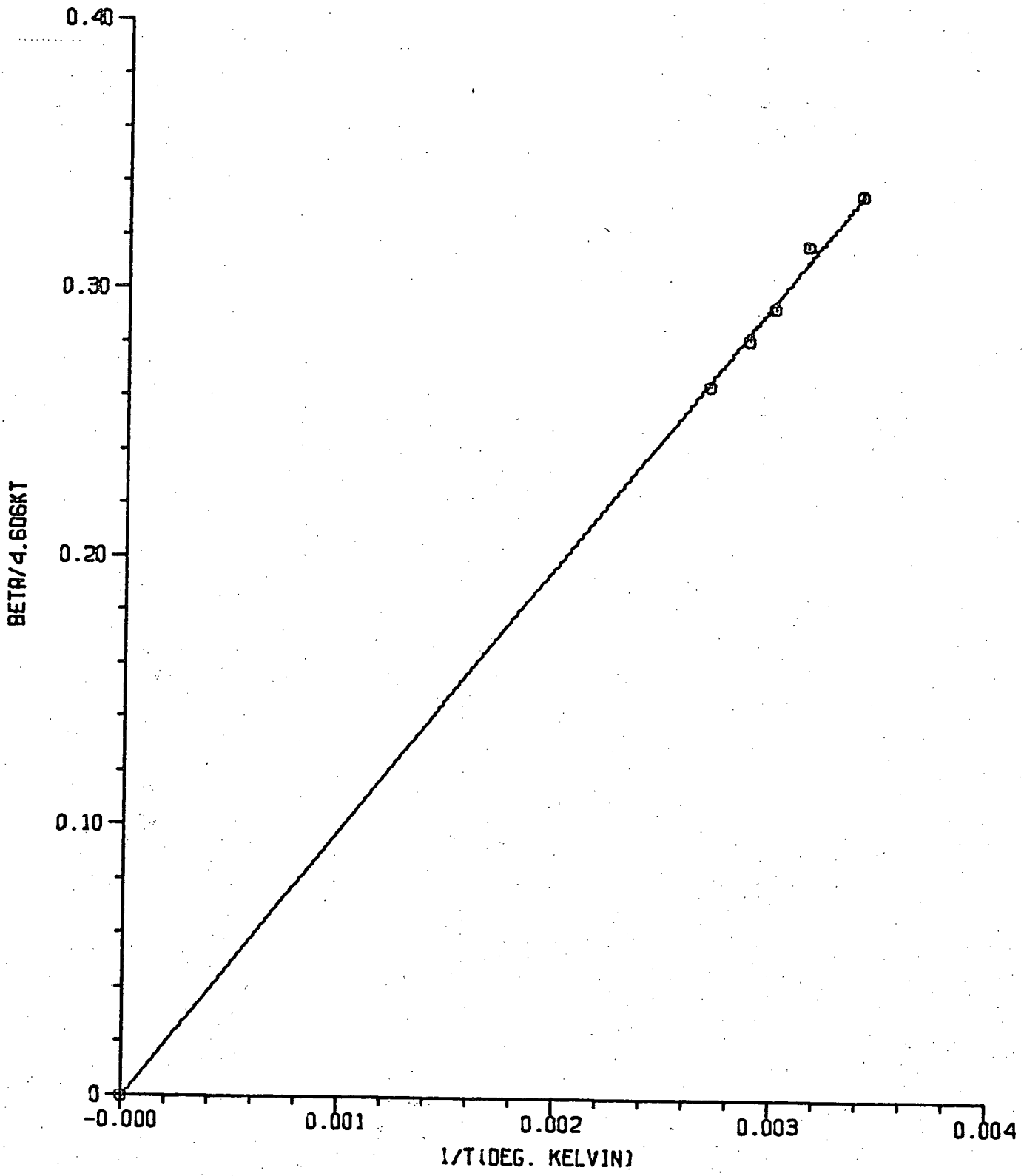
0.40
0.30
0.20
0.10
0
BETA/4.606KT
-0.000
0.001
0.002
0.003
0.004
1/T(DEG. KELVIN)

Fig. 10

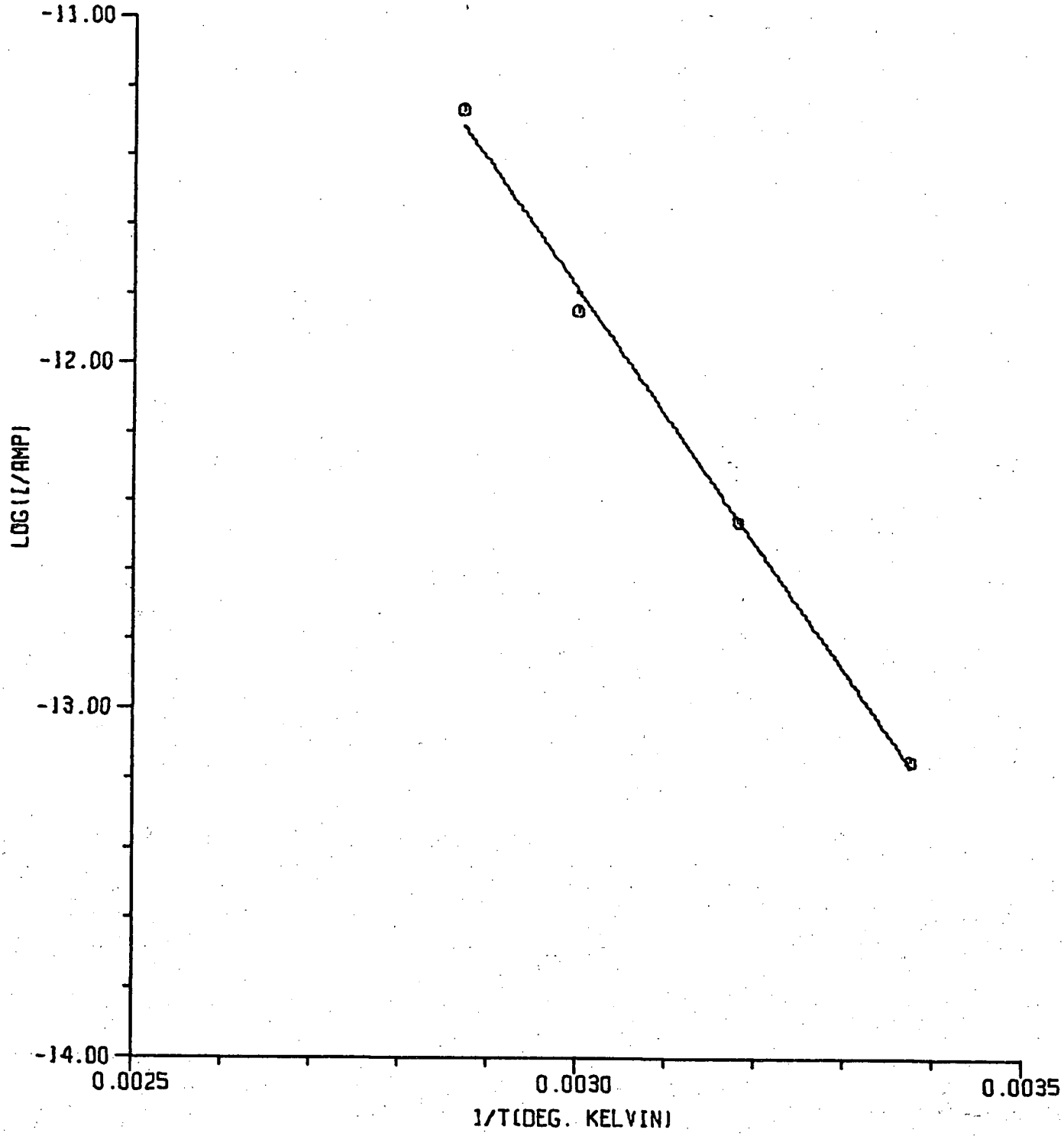

Fig. 11

Determination of Activation Energy

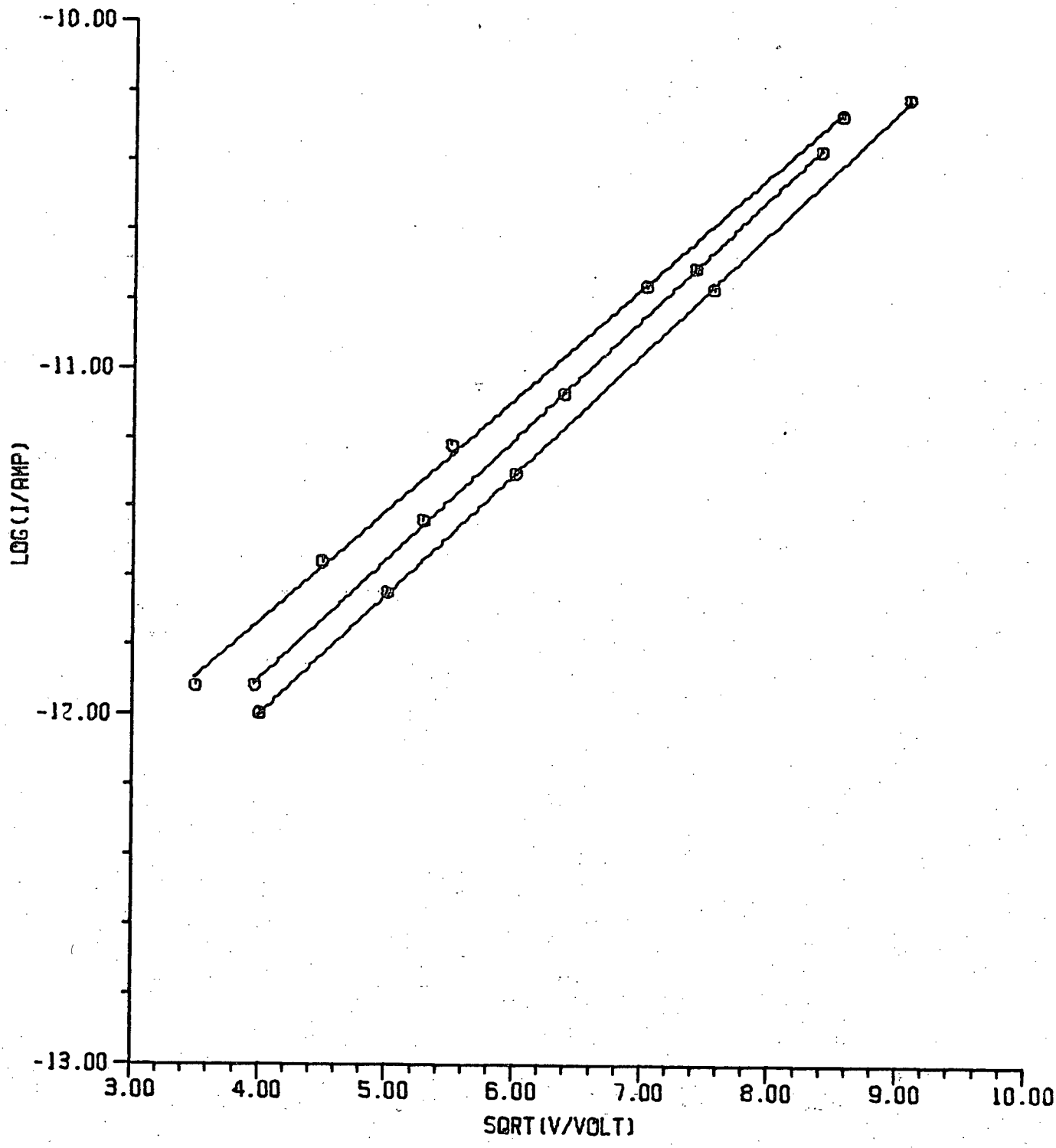

Fig. 12

Reproducibility of D.C. Conduction Current (P=50μHg)

Poole-Frenkel emission process dominates.

The possibility of ionic conduction was considered. However, the movement of different ions through Y_2O_3 would be expected to give different currents at the same potential. Fig. 7 showed that the electrode metal had little effect on the conduction process, so ionic conduction is unlikely.

Fig. 7 also eliminates Schottky emission as a possible conduction mechanism, since the different barrier heights at the two metal-insulator interfaces would give different currents for Schottky conduction, and this was not observed.

The most likely mechanism is Poole-Frenkel emission of electrons into the valence band from donor centers 0.6eV below the insulator conduction band. A fairly high concentration of oxygen vacancies or yttrium interstitials is possible, even though the films were evaporated in an oxygen ambient. Baking the films reduced the dielectric losses, probably by the filling of vacancies by diffusion of oxygen through the films. Hass et al[5] found, in the course of their work on optical properties of rare earth films, that only films deposited on a heated substrate did not change properties on subsequent baking. They attributed this to reduction of the oxide during evaporation onto cold substrates (as were used in this work). They found that baking reduced the optical absorption coefficient, but not to the value obtained for films deposited on heated substrates. Thus, both yttrium interstitials (unaffected by baking) and oxygen vacancies (partly filled by baking) are probably present in the partially reduced cool-substrate films. The slow drift in the film properties with time observed for electron beam evaporated Y_2O_3 films can also be explained by the slow filling of vacancies with oxygen atoms.

Contamination by cruicible material is an unlikely source of donors. The boron nitride crucible was held in a water-cooled block and hence was unable to reach the very high temperatures necessary for evaporation. Substantial contamination with substrate material is also unlikely, since these were Corning 7059 aluminosilicate glass, which has a low concentration of mobile alkali ions.

The pressure dependence of the Y_2O_3 conduction characteristics is not easily understood.

Berard et al[6], in their work on oxygen diffusion in single crystal rare earth sesquioxides found that Y_2O_3 has a high oxygen diffusivity (6.06×10^{-6} cm^2/sec) and a low activation energy (0.85eV).* They explained these results by a migration mechanism based on the inherently defective nature of the anion sublattice of these materials. As discussed in Chapter II, pathways exist in the Y_2O_3 crystal structure along which oxygen ions can migrate readily. The unusually open anion sublattice provides ample sites for the solution of interstitial oxygen. In determining the diffusion constant of oxygen in Y_2O_3, Berard assumed full solubility of oxygen in the crystal lattice, since no data were available on the solubility of oxygen in Y_2O_3. The diffusion constant could be several orders of magnitude higher, and in polycrstalline evaporated films, the porosity would make diffusion even easier. Assuming Berard's worst-case values gives the following results for diffusion for 1000 seconds at room temperature:

$$D = D_o \exp\left(-\frac{W}{kT}\right)$$

$$\sim 10^{-19}$$

$$x = \sqrt{Dt} \sim \sqrt{10^{-19} \times 10^{+3}} \text{ cm}$$

$$= 1\text{Å}$$

* Measured at a temperature of 1200°C.

However, if Berard's diffusion constant is too low by two orders of magnitude (as he indicated to be possible) and the average activation energy in the thin films is 0.6eV rather than 0.85eV, the diffusion distance becomes

$$x \sim \sqrt{6 \times 10^{-16} \times 10^{3}} \text{ cm}$$
$$= 7700 \text{ Å},$$

or more than the film thickness. Thus, oxygen diffusion cannot be eliminated as a possible cause of the reduced conductivity at lower pressures. Tallan and Vest[17], in their high temperature (1400-1800°C) measurement of the conductivity of bulk polycrystalline Y_2O_3 found that the material was an amphoteric semiconductor. The region of predominant hole conduction had the conductivity

$$\sigma = 1.3 \times 10^{3} P_{O_2}^{3/16} \exp(-1.94/kT) \qquad (26)$$

They explained their results by assuming the presence of fully ionized Y vacancies. In the films studied here, the trap density for holes is probably too great for hole conduction to occur. Also, yttrium interstitials are more likely to be present than yttrium vacancies. They did observe a strong dependence of σ on the oxygen partial pressure, as observed in this work.

The donor centers from which Poole-Frenkel emission occurs are probably interstitial yttrium atoms. The conduction process is likely determined by the interaction of yttrium interstitials, oxygen vacancies and dissolved oxygen atoms. Reducing the oxygen partial pressure would reduce the number of oxygen atoms in solution and increase the number of oxygen vacancies, and this may be the cause of the conductivity change with pressure. The presence of more oxygen vacancies, which act as deep electron

traps, would reduce the number of electrons in the donor levels available for Poole-Frenkel emission. If oxygen vacancies and yttrium interstitials are closely associated as neutral defect pairs, the presence of N_T deep traps (oxygen vacancies) would reduce the number of donors available for emission from N_D to

$$n_D = N_D - N_T \tag{27}$$

Then equation (21) would be modified to

$$J = e\sqrt{\frac{(N_D-N_T)\mu\nu\ E}{S}}\ \exp-\{\frac{(E_C-E_D)-\beta_{PF}\sqrt{E}}{2kT}\} \tag{28}$$

The empty donors produced by N_T vacancies would not act as trapping centers because of their close association with oxygen vacancies, so that the arguments leading to equation (21) are still valid.

Equation (28) does predict a lower conductivity at reduced oxygen partial pressures, assuming sufficiently rapid oxygen diffusion.

However, (28) does not explain the high value of the permittivity found at low pressures from the conduction data (11.7 vs. 3.2 at atmospheric pressure). It is likely that the reduced concentration of oxygen atoms and the increased oxygen vacancy concentration at low pressure caused some change in the refractive index of the oxide, but a change of the magnitude observed seems doubtful.

The Y_2O_3 films were found to have conduction characteristics quite similar to those of SiO thin films[14,15]. Both have bulk-limited conduction characteristics that fit the equation

$$I = I_o\ \exp-(\frac{W-\beta\sqrt{V}}{2kT})$$

A comparison is made in the following table:

TABLE 1

MATERIAL	Activation Energy W	n^2	I at E = 3×10^5 V/cm.
SiO	0.4eV	3.6	10^{-5} amps.
Y_2O_3	0.6eV	3.05	10^{-8} amps.

Y_2O_3 has much smaller conduction currents at the same electric field. The higher activation energy and different doping levels are likely the cause of this difference.

V. STEP RESPONSE AND LOSS FACTOR IN Y_2O_3

1. Introduction

The transient currents produced by the response of a dielectric material between conducting electrodes often yields useful information about low frequency losses in the material and the nature of the processes responsible for those losses. If $\phi(t)$ is the relaxation function of a material after application of a step in the potential across it, the real and imaginary parts of the complex permittivity can be expressed by[18]

$$\varepsilon'(\omega) = C_a^{-1}\{\int_o^\infty \phi(t)\cos\omega t\, dt + C_o\} \tag{1}$$

$$\varepsilon''(\omega) = C_a^{-1}\{\int_o^\infty \phi(t)\sin\omega t\, dt + G\omega^{-1}\}, \tag{2}$$

where $C_a \equiv$ capacitance with vacuum between the capacitor plates,

$C_o \equiv$ capacitance at high frequencies,

$G \equiv$ steady-state D.C. Conductivity,

and $\omega \equiv$ angular frequency.

These equations are general, except for the reasonable assumption that linear superposition holds for the observed currents in the material.

It has been found that a relaxation function of the form $\phi(t) = AC_a t^{-m}$ holds for many materials at a fixed temperature[19]. Use of this expression in (2) yields, after a contour integration convergent for $2 > m > 0$,

$$\varepsilon''(\omega) = [\omega^{m-1}A\Gamma(1-m)\cos(m\pi/2)] + G/\omega C_a, \tag{3}$$

For materials with a Cole-Cole* distribution of relaxation energies,

*The Cole-Cole distribution function has the form[20]

$$F(s)ds = \frac{1}{2\pi}\,\frac{\sin a\pi}{\cosh(1-\alpha)s - \cos a\pi}\,ds,$$

where a and α are constants. The distribution is similar to the Gaussian distribution, but it is less peaked. Many materials have a Cole-Cole distribution of relaxation times.

the permittivity has been determined to be

$$\varepsilon = \varepsilon' - j\varepsilon'' = \varepsilon_\infty + \{(\varepsilon_o - \varepsilon_\infty)/[1+(j\omega\tau_o)^n]\} \tag{4}$$

Here the high-frequency dielectric constant is $\varepsilon_\infty = \frac{C_o}{C_a}$, ε_o is the static dielectric constant, τ_o is the most probable relaxation time and $n = 1 - \alpha$, where α is a factor determining the distribution width. Both n and α vary between 0 and 1.

The reversible transient current $\phi(t)$ flowing at a time t after a step in voltage can be found by taking the inverse Fourier transform of (1) and (2) giving

$$\phi(t) = \frac{1}{\pi} \int_o^\infty \varepsilon(j\omega) \exp(j\omega t) d\omega \tag{5}$$

On substitution of (4) into (5), expanding in a series and integrating, two limiting cases arise:

$$\phi(t) = [(\varepsilon_o - \varepsilon_\infty)/\tau_o][1/\Gamma(n)](t/\tau_o)^{-(1-n)} \tag{6}$$

for $t \ll \tau_o$, and

$$\phi(t) = [(\varepsilon_o - \varepsilon_\infty)/\tau_o][n/\Gamma(1-n)](\frac{t}{\tau_o})^{-(1+n)} \tag{7}$$

for $t \gg \tau_o$, where τ_o is a characteristic time. Hence, for a given material the log $\phi(t)$ vs. log (t/τ_o) curve has a slope of

$$s_1 = -(1-n) = -\alpha \tag{8}$$

for times short compared to the most probable relaxation time τ_o, and a slope of

$$s_2 = -(1+n) = -(2-\alpha) \tag{9}$$

at times very long compared to τ_o. At times near τ_o, the curve bends over. This is the dispersion region where a peak in ε'' occurs.

The dielectric loss factor for a Cole-Cole distribution has been found

for the two limiting cases to be

$$\varepsilon''(\omega) = (\varepsilon_o - \varepsilon_\infty)(\omega\tau_o)^n \sin(n\pi/2) \tag{10}$$

for $(\omega\tau_o) << 1$, and

$$\varepsilon''(\omega) = (\varepsilon_o - \varepsilon_\infty)(\omega\tau_o)^{-n} \sin(n\pi/2) \tag{11}$$

at high frequencies where $\omega\tau_o >> 1$.

2. Experimental Procedures

Step response measurements were carried out with the same circuit used for conduction measurements, except for the addition of a switch. Currents were measured with the Keithley 417 high-speed picoammeter. The time constant of the picoammeter input circuit was small compared to the current decay rates measured for the current ranges used.

Capacitance and loss measurements were made with a General Radio 1615-A capacitance bridge in the three-terminal mode. Measurements were made in the 100 Hz-100kHz frequency range.

3. Results

3.1 Step Response

Typical results for charging and discharging currents are shown in the double log plots of Fig. 1 and 2 for an yttrium oxide film 1250 $\pm$ 50 Å thick. The counterelectrode metals were aluminum and indium. The two plots are very similar for the same voltage step, except that the D.C. conduction current eventually dominates the charging characteristic.

In Fig. 3, a plot is made of $\log(I/I_o)$ against $\log(t/\tau_o)$ for discharge currents after a voltage step of 3 volts. I_o and τ_o are the current and time at the point where the 3 volt curve in Fig. 2 bends over. From Fig. 3, the slopes determined in the two regions are

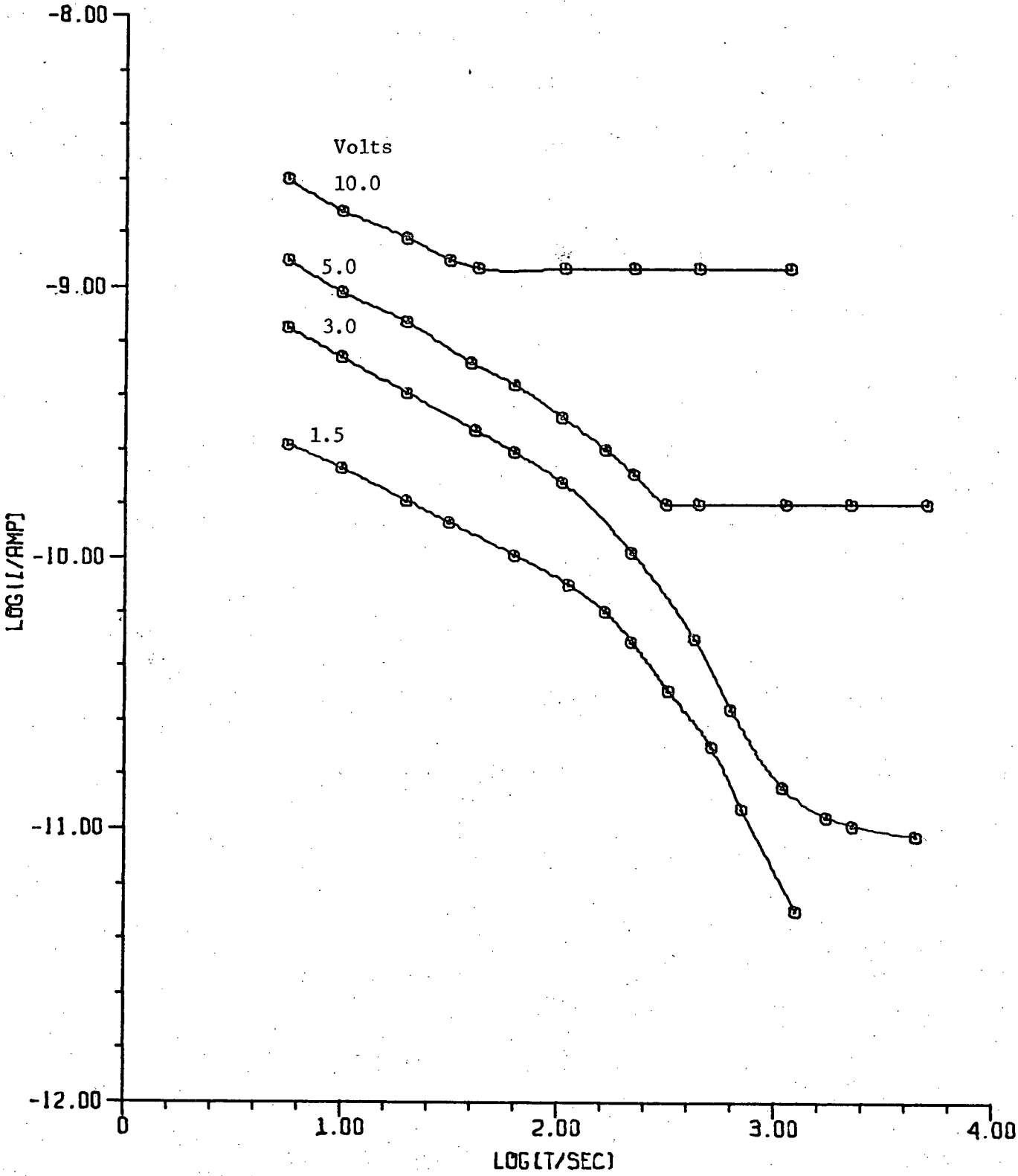

Fig. 1

Al-Y_2O_3-Al Step Response Charging Current

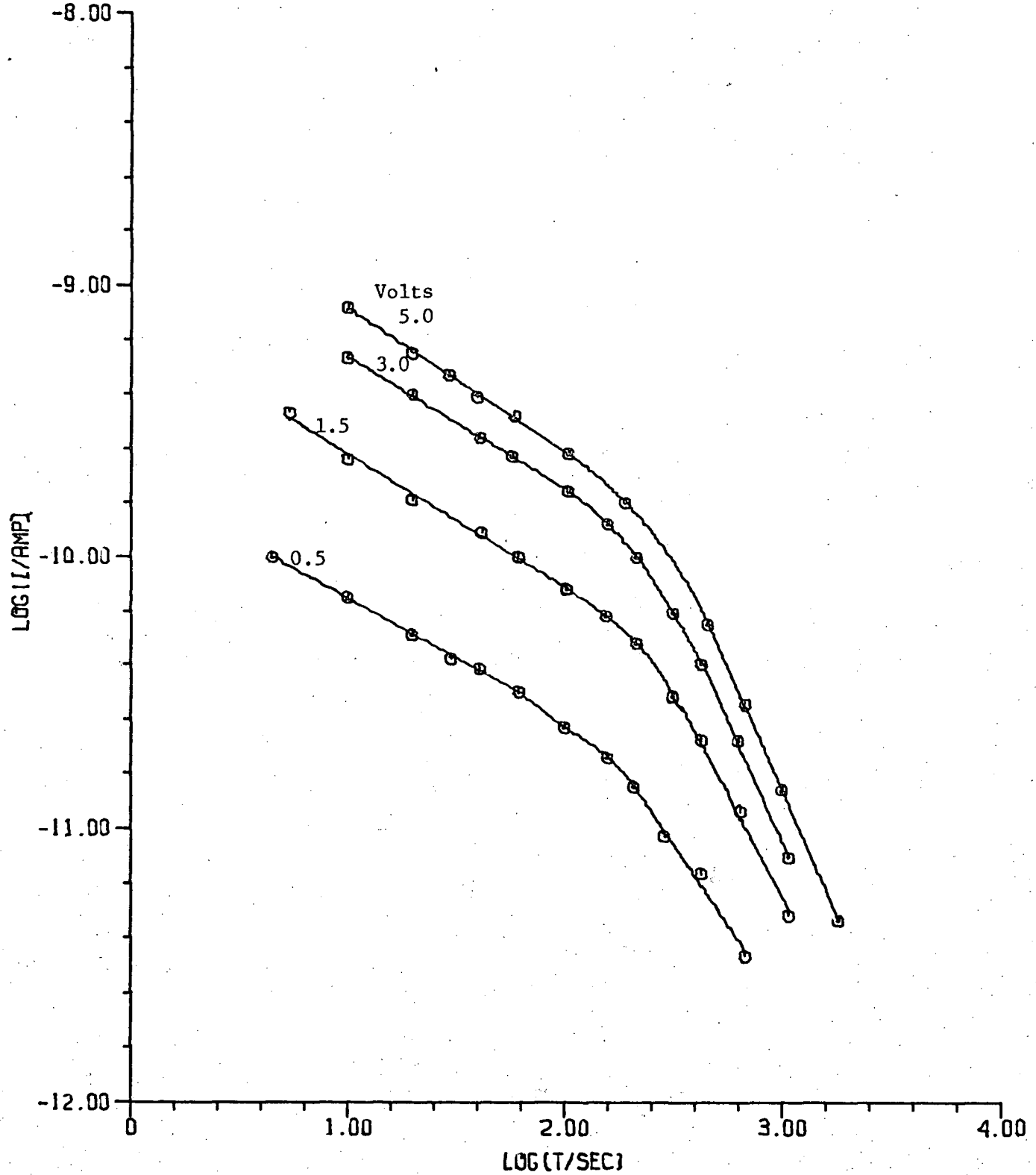

Fig. 2

Al-Y_2O_3-Al Step Response Discharging Current

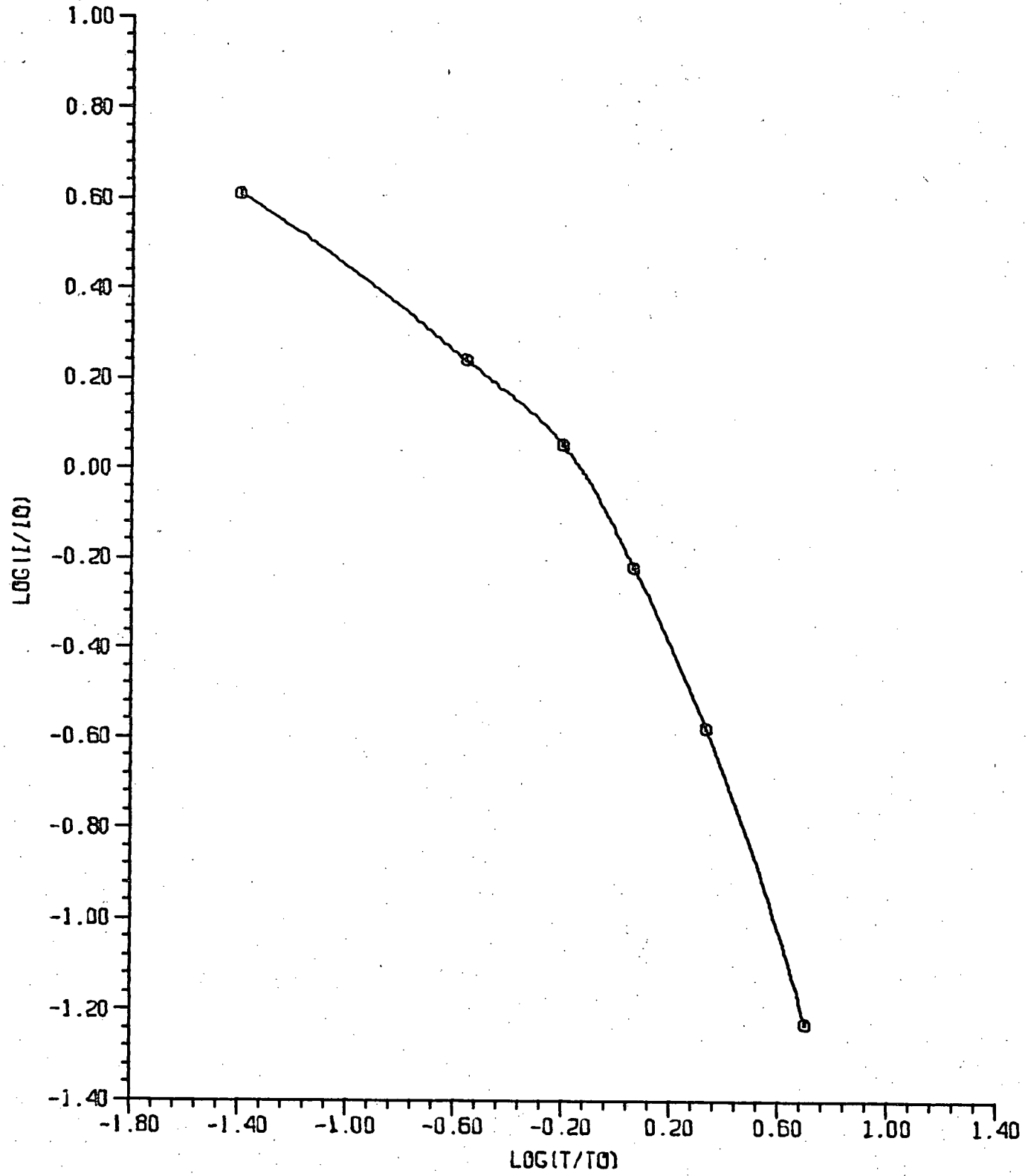

Fig. 3

$\text{Log}(\frac{I}{I_o})$ vs. Log $(\frac{t}{\tau_o})$ For Discharge After 3V Step.

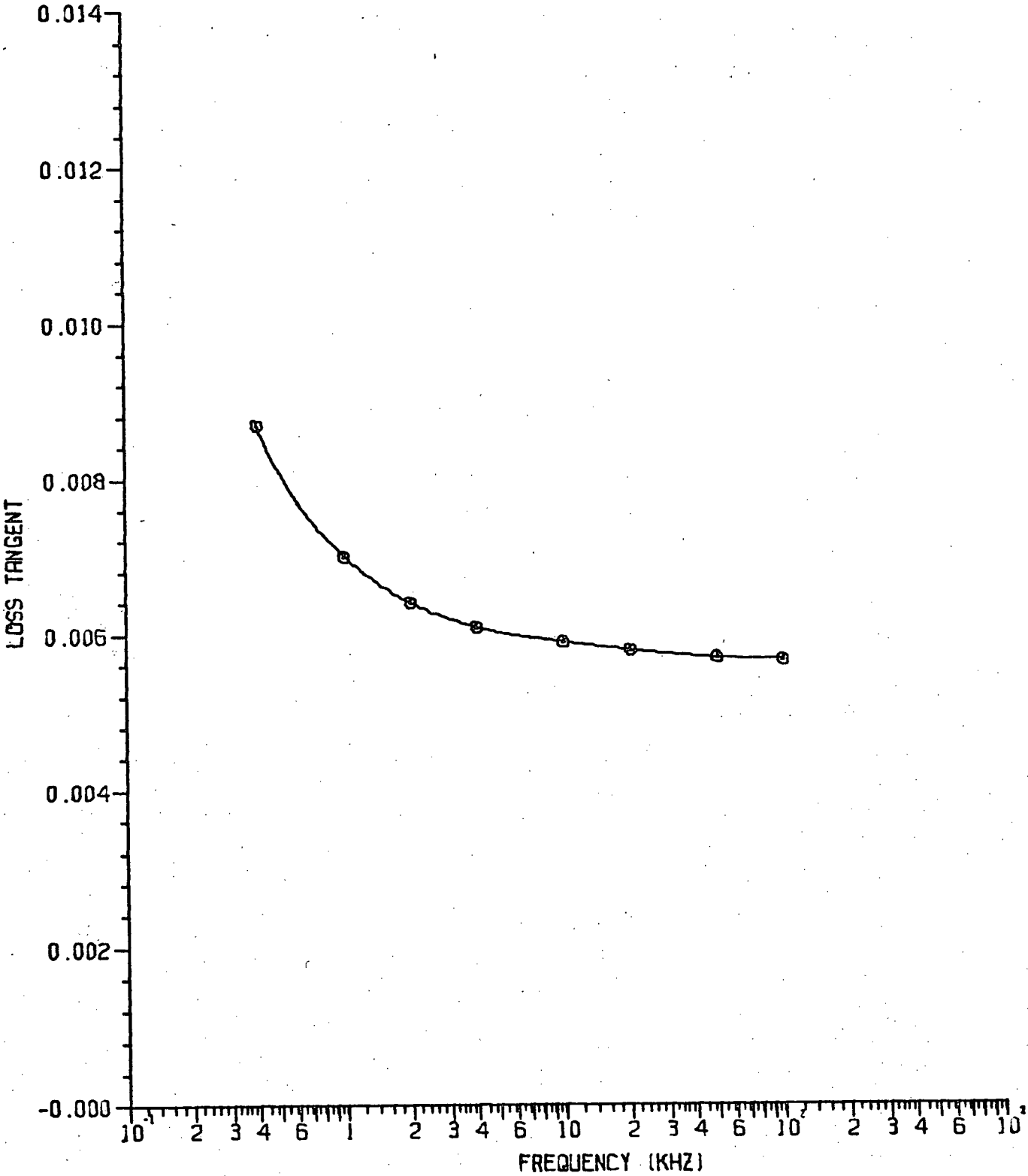

Fig. 4

Dielectric Losses vs. Frequency

$$s_1 = -0.49 \pm 0.03 \quad \text{for } t \ll \tau_o$$

and $s_2 = -1.49 \pm 0.03$ for $t \gg \tau_o$. Use of equations (8) and (9) gives an average value for n of 0.50 ± 0.03. The characteristic time τ_o was 200 seconds.

Use of the following parameters in equation (11) gives the variation of the high-frequency dielectric loss with frequency:

$\varepsilon_\infty = 3.05 \pm 0.02$ (optical measurements)

$\varepsilon_o = 12.4 \pm 1.0$ (capacitance measurements)

$n = 0.50 \pm 0.03$

$$\varepsilon''(f) = \frac{0.186}{\sqrt{f}} \pm 10\%. \tag{12}$$

3.2 Loss Factor

The dielectric loss factor for a Y_2O_3 film 1950 ± 80 Å thick with indium and aluminum counterelectrodes is shown in Fig. 4. This result is similar to that found by Campbell[1] for Y_2O_3 films, although the magnitude of his dissipation factor was somewhat smaller at low frequencies.

4. Discussion

The agreement between the loss factor calculated from step response measurements and that determined by bridge methods was only approximate. This suggests that two different loss mechanisms are operative.

The mechanism responsible for the step response losses is likely field-assisted thermal hopping of oxygen atoms between interstitial sites in the Y_2O_3 lattice. The step response data fit a model that has a Cole-Cole distribution of relaxation energies. An estimate of the most probable relaxation energy can be made using

$$\tau_o = \nu^{-1} \exp(E_p/kT) \tag{13}$$

where $\tau_o \equiv$ most probable relaxation time

$\nu \equiv$ atomic vibration frequency

$E_p \equiv$ most probable relaxation energy.

A reasonable estimate for ν from optical phonon spectra is 10^{13} Hz at room temperature.

This gives $E_p \simeq 0.91$eV.

A comparison can be made with the diffusion results of Berard et al (1968) who found an activation energy of 0.85 eV for the diffusion of oxygen atoms in Y_2O_3. Considering the nature of the approximations made, the agreement between the two activation energies is quite good. Thus, the loss peak may be due to the relaxation of oxygen atoms dissolved in the Y_2O_3 lattice.

Campbell (1970) found a strong dependence of dielectric losses on temperature in his Y_2O_3 films. He felt that this dependence was indicative of an activation energy process, but for the temperatures considered (between 20 and 75 ^oC), the steep frequency dependence of ε'' precluded a flat distribution of activation energies. The proposed loss mechanism is in agreement with these conclusions.

At higher frequencies, the losses were independent of frequency, indicating that a different loss mechanism is dominant. This view is supported by the poor agreement between the measured values of ε'' and the calculated values predicted by the theory in the introduction at high frequencies.

The slightly higher high frequency losses found in this work (0.058 compared to 0.038 found by Campbell) may be caused by the use of different substrates or some small difference in evaporation technique.

VI. BARRIER HEIGHT DETERMINATION BY INTERNAL PHOTOEMISSION

1. Introduction

Internal photoemission is the emission of photoexcited carriers over the energy barrier at the interface between a metal (or semiconductor) and an insulator. From photocurrent measurements as a function of the wavelength of incident light, the energy barrier height may be determined.

Fowler[21] has given an approximate classical treatment of the photoelectric effect (emission of electrons from a metal into vacuum). The exact quantum mechanical theory is given by Mitchell[22]. For the purposes of this work, the two treatments give essentially identical results, so the simpler theory of Fowler will be referred to.

Consider the simplified energy band structure of a metal-insulator-metal diode shown in Fig. 1.

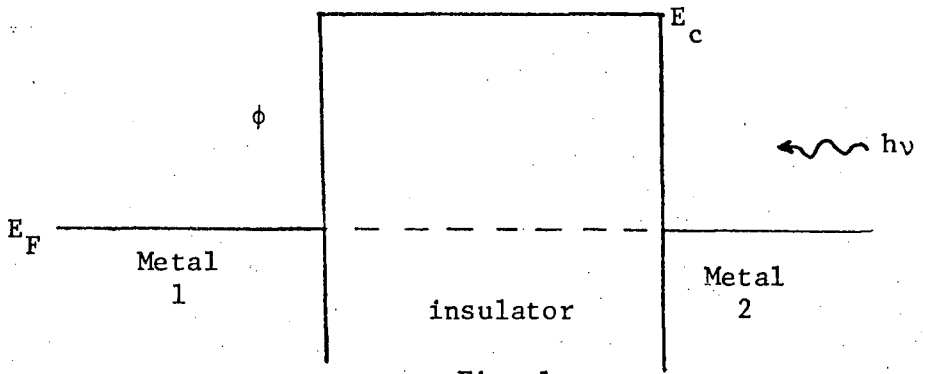

Fig. 1

The effective work function ϕ is the difference in energy between the Fermi level and the insulator conduction band. Electrode 2 is very thin and hence semi-transparent. For an electron to be excited from metal 1 into the insulator conduction band by an incident photon of energy $h\nu$, the condition

$$h\nu + E > \phi \tag{1}$$

must be met. E is the initial kinetic energy of the electron. The lowest

photon energy for emission is given by

$$h\nu = \phi, \tag{2}$$

which defines the photoelectric threshold.

For electron emission, the energy $\frac{p^2}{2m}$ of the electron motion perpendicular to the emitting surface should exceed ϕ. In a first approximation, the other velocity components may be neglected. The condition for emission may then be expressed as

$$\frac{p^2}{2m} + h\nu > \phi \tag{3}$$

The photoelectric yield is expected to be proportional to the incident light intensity, the number of electrons meeting condition (2), the chance that the quantum $h\nu$ will be absorbed by the electron velocity component normal to the metal surface, and the probability that the electron will be transmitted through the barrier at the metal insulator boundary. Fowler, using these assumptions, found that the photoresponse R (electrons per incident photon) was given by

$$R = \frac{4\pi m k^2 T^2}{h^3} \{e^x - \frac{e^{2x}}{2^2} + \frac{e^{3x}}{3^2} - \ldots\} \tag{4}$$

for $x = (\frac{h\nu-\phi}{kT}) \lesssim 0$, and

$$R = \frac{4\pi m k^2 T^2}{h^3} \{\frac{\pi^2}{6} + \frac{x^2}{2} - (e^{-x} - \frac{e^{-2x}}{2^2} + \frac{e^{-3x}}{3^2}) - \ldots\} \tag{5}$$

for $x \gtrsim 0$.

For large values of x (say $x > 8$, a value easily met in practise), the only significant term in the expansion is $\frac{x^2}{2}$ in (5). Thus, the photocurrent expected is

$$I = C(h\nu - \phi)^2 \tag{6}$$

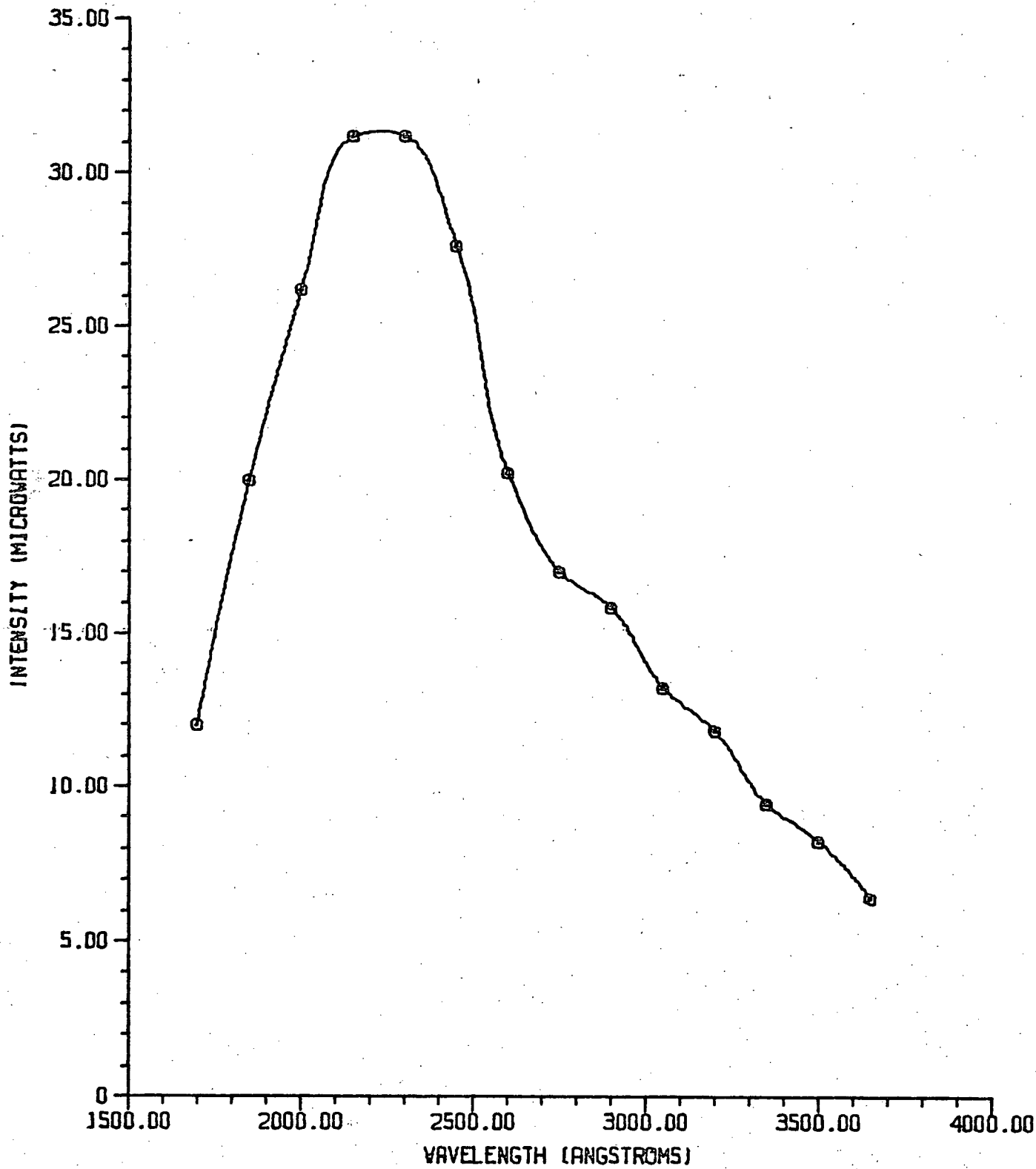

Fig. 2

Monochromator Calibration Curve (Deuterium Source)

where C is a constant. A plot of the square root of the current against the photon energy hν will give a straight line for large values of x.

In the presence of an electric field, the barrier height will be lowered by

$$\Delta\phi = \sqrt{\frac{e\,E}{4\pi\epsilon}} \tag{7}$$

because of the Schottky effect.

2. Experimental Procedures

The photocurrents were measured with the circuit shown below.

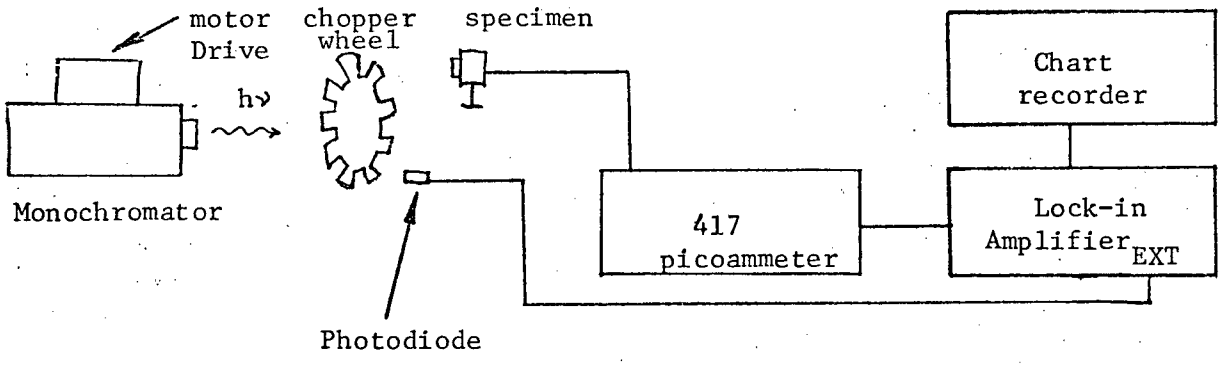

Light from the Bausch and Lomb precision grating monochromator was chopped at a frequency of 2 2/3 Hz. This low frequency was used because of the long time constant of the picoammeter input in its most sensitive range. The currents developed in the specimen were detected by the Keithley 417 picocammeter, amplified in the Princeton HR-8 lock-in amplifier and plotted on a Moseley chart recorder. The lock-in amplifier was used in the selective external mode, with the external signal being derived from the output of a photodiode in the path of the chopped light. This method of detection was found superior to the D.C. method because errors due to slow transient currents in the dielectric film were eliminated, as were some of the noise problems associated with measuring currents of less than

10^{-10} amperes. The setup was capable of detecting currents as small as 2×10^{-14} amperes, but the smallest currents capable of being measured in Y_2O_3 were about 5×10^{-12} amperes because of noise limitations.

The monochromator had a choice of two light sources and three gratings capable of covering the entire wavelength spectrum from 200 millimicrons to 3.6 microns.

A calibration of the source intensity was made by illuminating an Eppley* silver-bismuth thermopile with light from the monochromator. Chopping the light was found to reduce the average intensity by a factor of 2. Photoemission measurements were made with the specimen in the same position as the thermopile. The thermopile voltages were measured with a Keithley 150 A microvoltmeter and recorded with a Moseley chart recorder. A synchronous 1 RPH motor was used to drive the monochromator diffraction grating. A typical run took 45 minutes. The slow scan rate eliminated slow transient effects from the data.

The monochromator entrance and exit slits were set at 2.78 and 1.56 mm. width. This permitted a band of wavelengths 10 millimicrons wide to pass through the monochromator. Narrower settings gave better spectral purity, but the light intensity was too low.

3. Experimental Results

The sensitivity of the thermopile used to make light intensity measurements was 19.0μW/μV.

Fig. 2 shows the spectral variation of the monochromator in the ultraviolet region. The deuterium light source was used. A similar calibration in the visible range is given in Fig. 3. The tungsten halogen lamp was the light source. The calibration curve for the spectral region of interest for

* Made by Eppley Laboratories, Newport R.I., U.S.A.

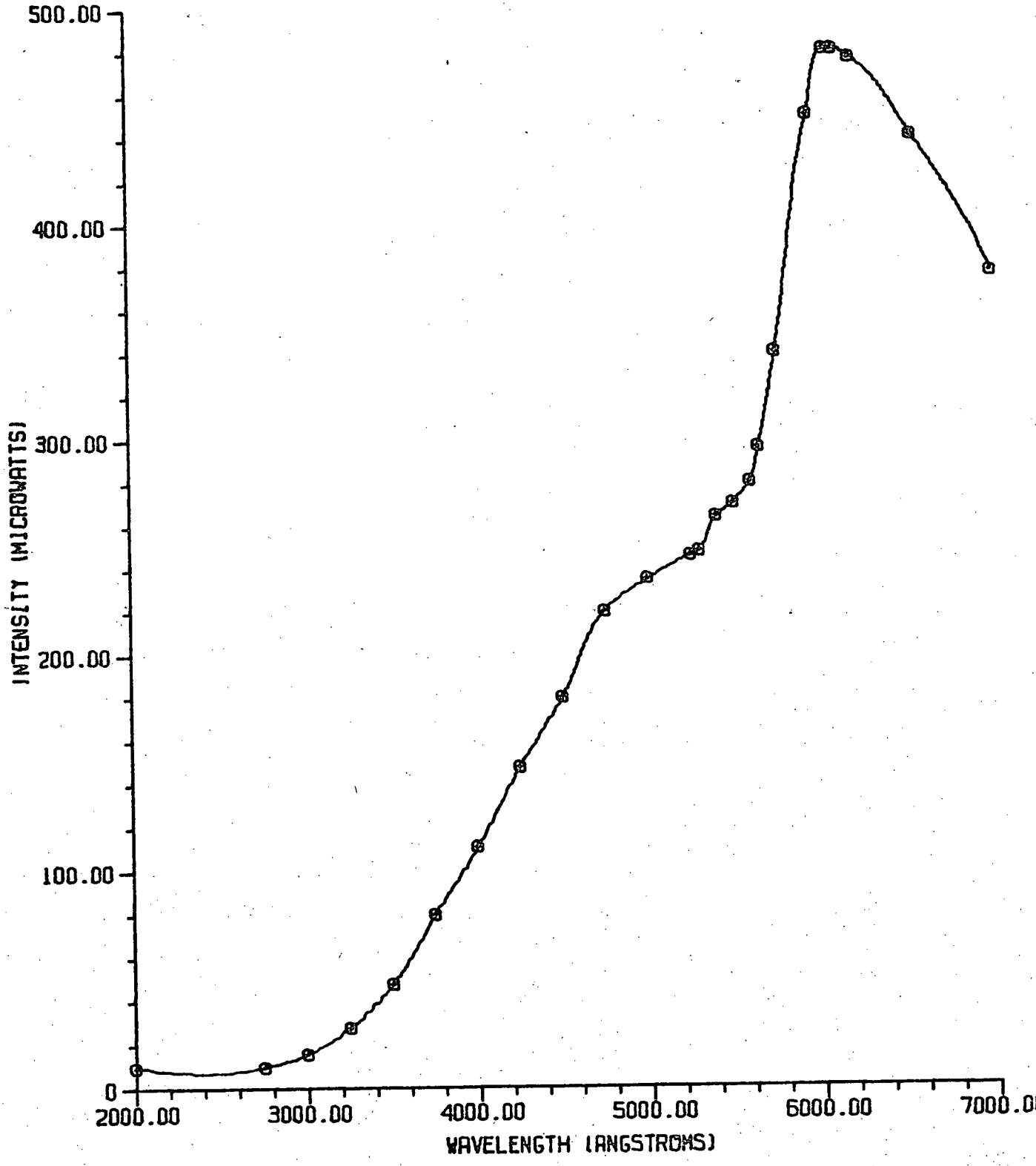

Fig. 3

Monochromator Intensity Calibration (Visible Range)

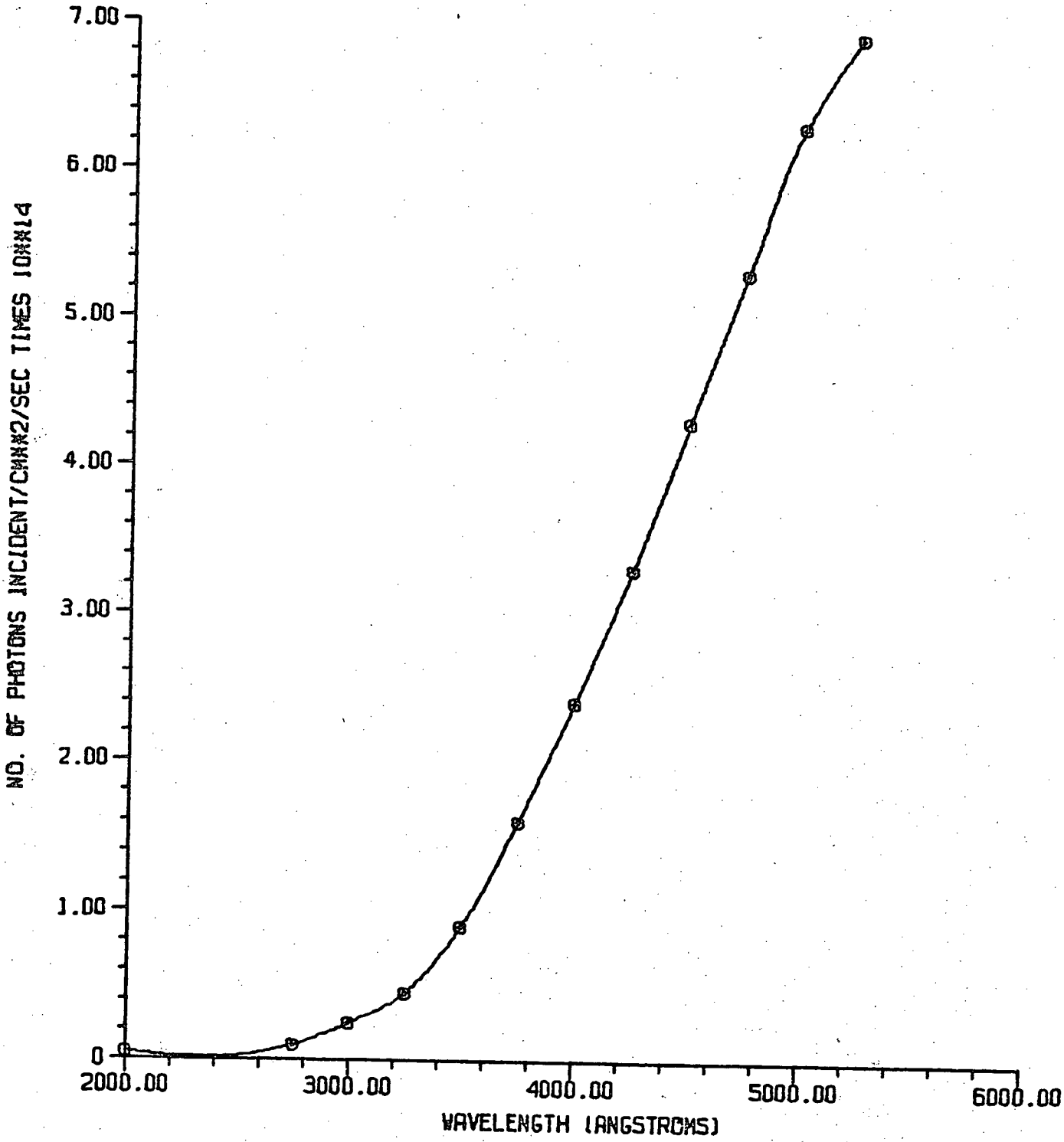

Fig. 4

Monochromator Calibration (2000-5000 A^{o})

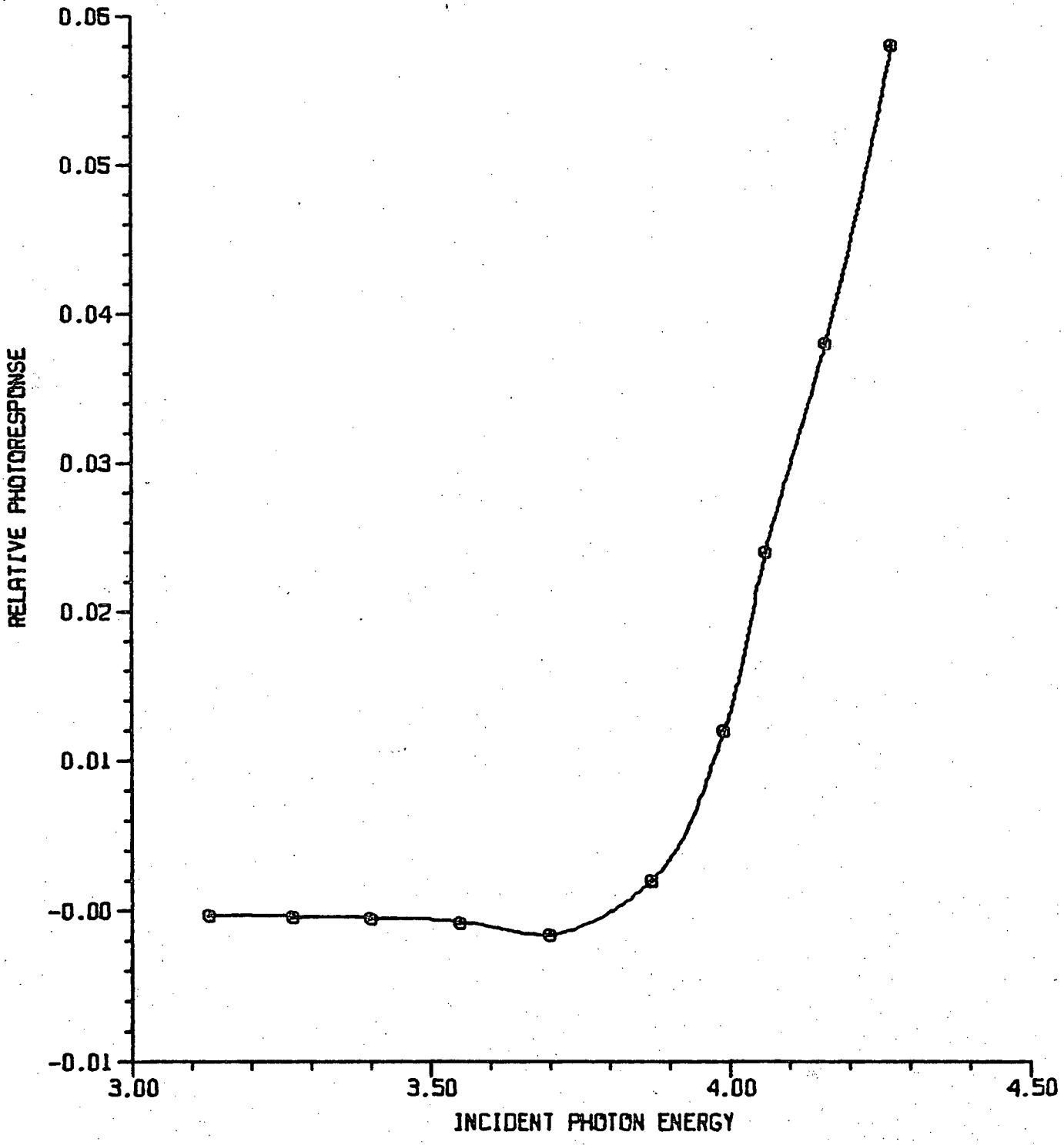

Fig. 5

Photoresponse of Al-Y_2O_3-Al

Y_2O_3 photoemission is shown in Fig. 4, which shows the incident photon flux.

Fig. 5 shows the photoresponse of an aluminum-yttrium oxide-aluminum MIM structure. The insulating film was measured to be 880 ± 100 Å with the Sloan M-100 Angstrometer. The aluminum counterelectrode was about 100 Å thick and had a transmission coefficient of 0.04 for white light.

The response was observed to first go negative, then positive with increasing ν. Since no potential was applied across the insulating film, the photoresponse must be due to two photocurrents, one from each electrode. Schuermeyer[23] has suggested that the photoresponse can be expressed as the sum of two currents of the Fowler type, giving

$$R = c_2(h\nu-\phi_2)^2 - c_1(h\nu-\phi_1)^2 \tag{8}$$

where the constants c_1 and c_2 are different because the light intensities are different in the two metal films. If $\phi_2 > \phi_1$, then for $h\nu < \phi_2$, $c_2 = 0$; similarly, for $h\nu < \phi$, $c_1 = 0$ also. For $\phi_1 < h\nu < \phi_2$,

$$\sqrt{|R|} = \sqrt{c_1}(h\nu-\phi_1) \tag{9}$$

The first points in the negative portion of Fig. 5 were plotted in Fig. 6 to give $\sqrt{J_1}$. The barrier height was found to be

$$\phi_1 = 3.14 \pm 0.06\text{eV}. \tag{10}$$

The positive current

$$\sqrt{J_2} = \sqrt{c_2}(h\nu-\phi_2) \tag{11}$$

was found using equation (8) and the result plotted in Fig. (6). The work function ϕ_2 was found to be

$$\phi_2 = 3.72 \pm 0.07 \text{ eV}. \tag{12}$$

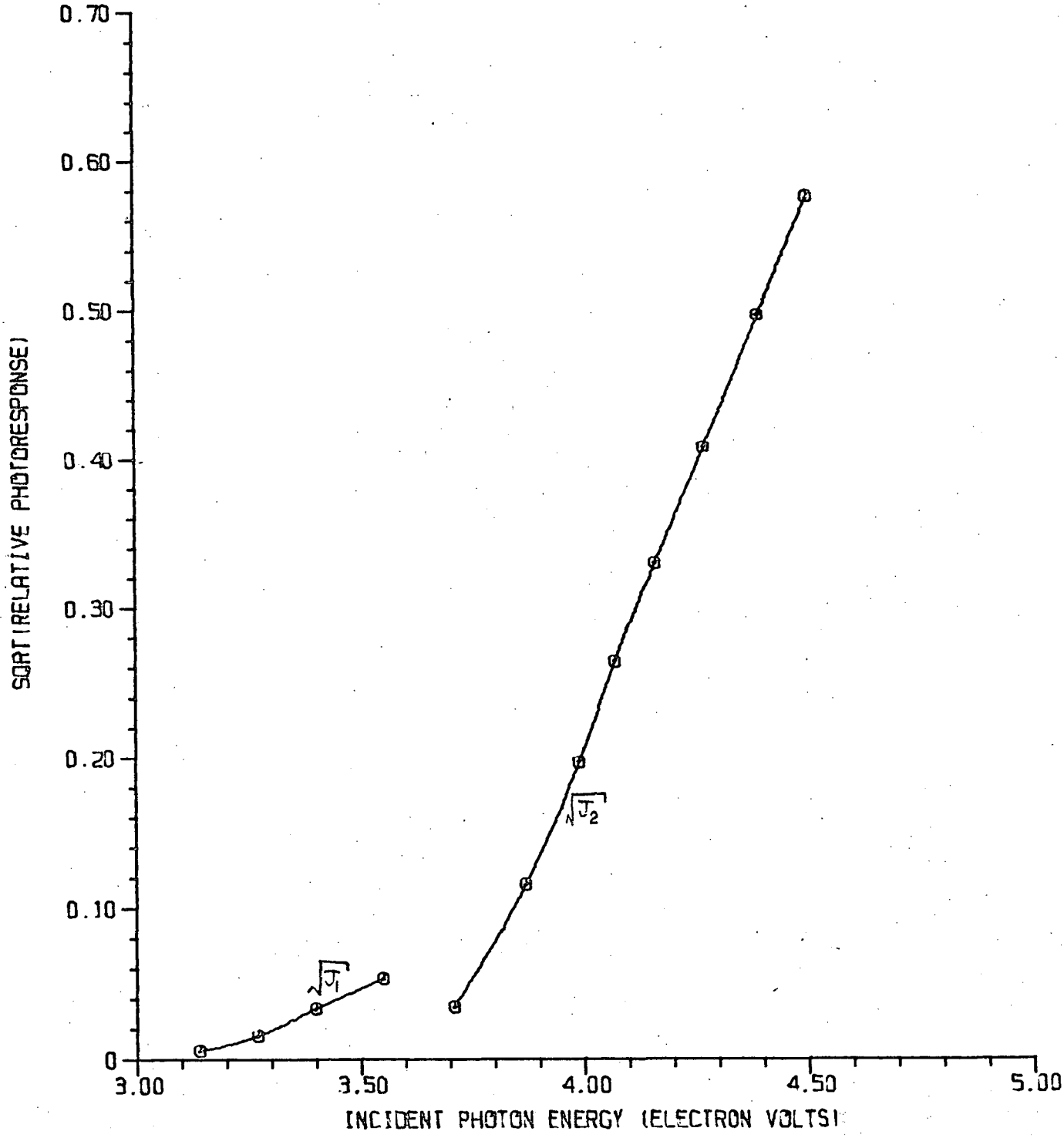

Fig. 6

Fowler Plots for Al-Y_2O_3-Al

The electric field in the insulator is

$$E = \frac{\phi_2 - \phi_1}{W}$$

$$= (6.7 \pm 2.2) \times 10^4 \text{ volts/cm.}$$

The Schottky barrier lowering is

$$\Delta\phi = 0.0056 \pm 0.00015 \text{ eV},$$

which is much smaller than the errors in ϕ_1 and ϕ_2, so it may be neglected.

4. Discussion

The barrier determined for Y_2O_3 was found to have the following shape:

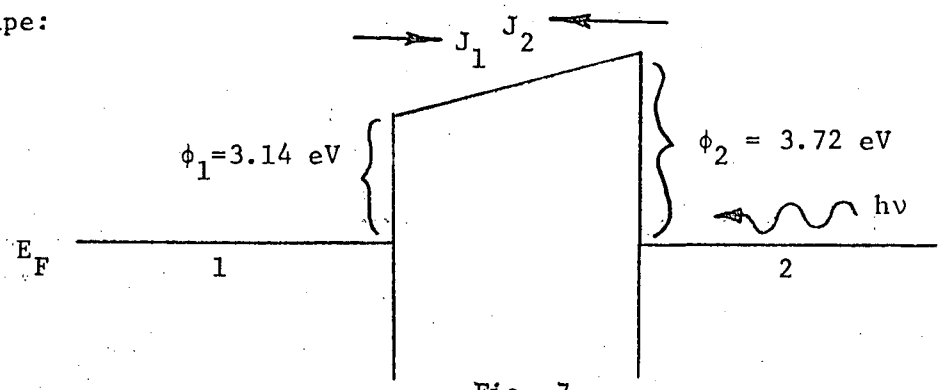

Fig. 7

A simple explanation of the observed currents can be given. For $\phi_1 < h\nu < \phi_2$, only J_1 flows in the insulator. Because the intensity of light in metal (1) is low, and because J_1 is attenuated by the electric field in the insulator, the current observed is small. When $h\nu > \phi_2$, both J_1 and J_2 flow, but J_2 rapidly becomes dominant because it is assisted by the intrinsic field and the intensity of light in metal (2) is large. In the region $h\nu \sim \phi_1$ or $h\nu \sim \phi_2$, a curvature is observed in the Fowler plot. This is due to the spread in the occupation probability of electron energy states near the Fermi level because the temperature is greater than absolute zero.

A more exact model would take other factors into account. When $h\nu > \phi$, the electrons will be injected into the oxide with the energy

$$E = \frac{p^2}{2m} + h\nu - \phi, \text{ where}$$

$\frac{p^2}{2m}$ was the initial electron kinetic energy with a momentum normal to the metal surface. The other components of momentum have been neglected, as was done in Fowler's derivation. When $h\nu - \phi$ is sufficiently large, the electrons injected will be hot electrons, which have different transport properties than thermal electrons. The interference of light between the metal electrodes must be taken into account, as it affects the intensity of light in the metal films. The absorption of light by the metal films must also be considered. The effects of scattering just inside the insulator may also be significant. Some of the injected electrons will simply be scattered back into the metal.

Some of these factors have been considered by a number of researchers[25,26,27,28], but no comprehensive model has yet been developed. The most promising results[26,27] have been obtained with Monte Carlo calculations of internal photoemission yields, which gave a good fit to experimental data on Al-Al_2O_3-Al.

The data obtained for Y_2O_3 appear to fit the simple model well, but the fairly large experimental errors would mask any second order effects. The barrier heights found are comparable to those found for other wide bandgap insulators. The difference in work functions at the two barriers is due to the preparation method. The first aluminum film was exposed for a short time to air and likely had about 50Å of Al_2O_3 on the surface. The other film was evaporated directly onto the Y_2O_3 film, so a different effective barrier height could result.

VII. CONCLUSIONS

The thin Y_2O_3 films investigated were found to have many of the properties essential for device fabrication.

The insulating properties of the films were excellent, and the evaporation of Y_2O_3 was a reasonably simple, non-critical process.

The ionic mobility was found to be quite high in the films, leading to low-frequency losses, and hysteresis in the MOS capacitance curves. It may be possible to improve the performance of the films by depositing on a heated substrate in order to prevent reduction of the evaporant.

A number of other experiments can be suggested. It would be desirable to know more about the pressure dependence of the conduction process in Y_2O_3, in order to check the mechanism proposed. Also, step response data taken at different temperatures would be useful. A plot of the most probable relaxation frequency against reciprocal temperature would then give a more accurate estimate of the mean activation energy of the loss mechanism.

Further investigation of the properties of Y_2O_3 in MOS structures would be desireable. In view of the ease of deposition, Y_2O_3 may be a useful material for double-dielectric device fabrication.

Further work on modelling the internal photoeffect is necessary, with particular emphasis on the hot nature of photoelectrons at light energies well above the photoelectric threshold.

APPENDIX

Preliminary investigation of the MOS capacitance curves of Au-Y_2O_3-Si devices showed hysteresis in the 1 MHz differential C-V curves. Figs. 1-3 were generated on an X-Y plotter by the application of a voltage of triangular waveform and low frequency across the specimen while measuring the MOS capacitance with a Boonton model 71A capacitance-inductance meter. The specimen had a Y_2O_3 film 1500 $\pm$ 200A° thick on n-type silicon of 0.4 $\pm$.05Ω -cm resistivity.

The hysteresis observed was more pronounced at lower scan frequencies. Comparison with the ideal MOS capacitance, as calculated using the MOS depletion approximation model[29], indicated a surface state density of about 3 x $10^{11}/cm^2$. This is surprisingly low, considering the high energies involved in the electron beam evaporation (i.e., x-rays) that would be expected to give higher defect densities and hence higher surface state densities. Thus, Y_2O_3 appears to be a useful material for MOS devices from surface state density considerations.

The hysteresis observed may be caused by the slow movement of either electronic or ionic charges near the Y_2O_3-Si interface. If ionic motion is the cause (as seems likely, considering the structure of the oxide films and the A-C losses observed), the motion of oxygen ions is probably the mechanism.

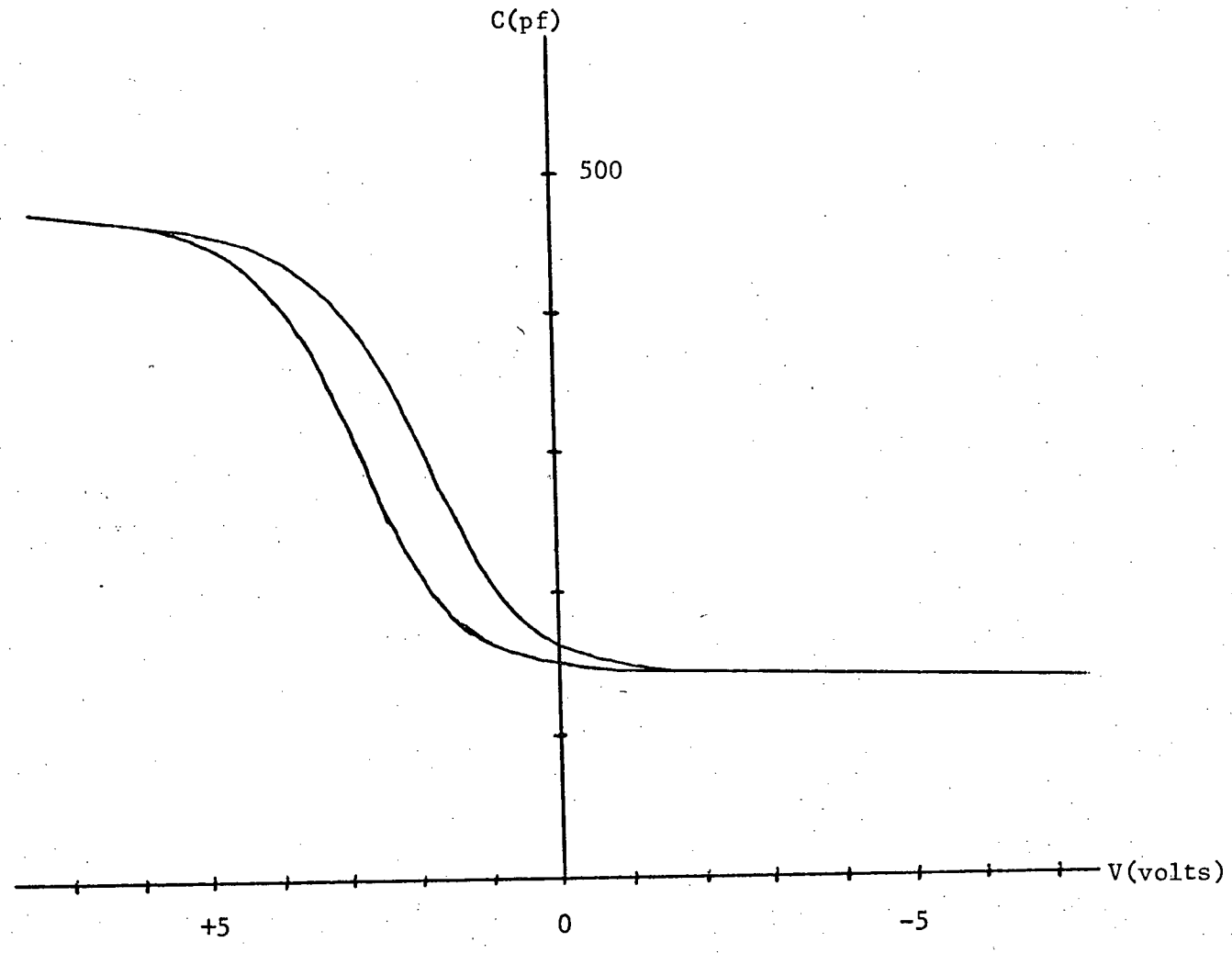

Fig. 1

MOS C Hysteresis (Sweep Frequency = 0.1 Hz)

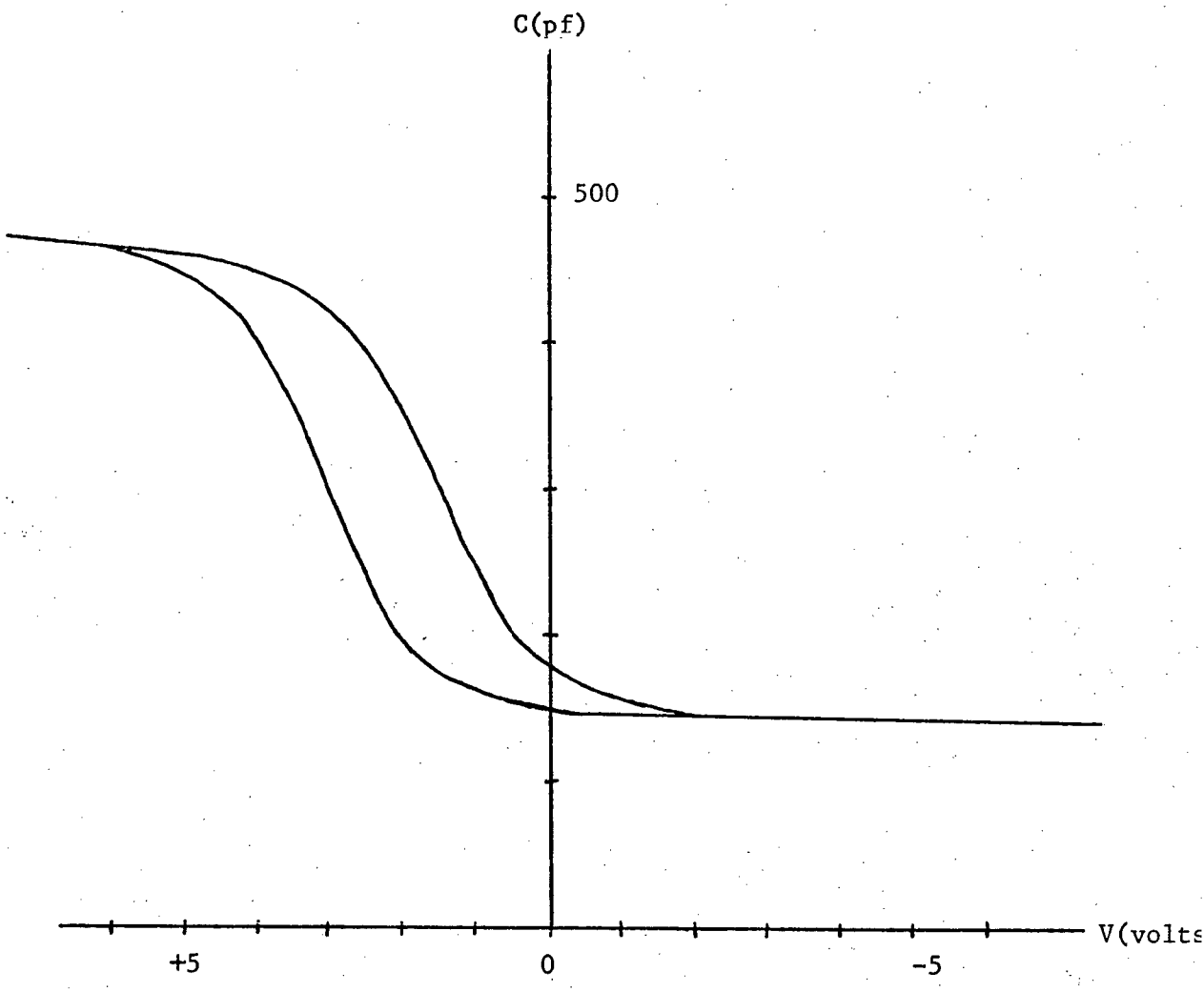

Fig. 2

MOS C Hysteresis (f = 0.05 Hz)

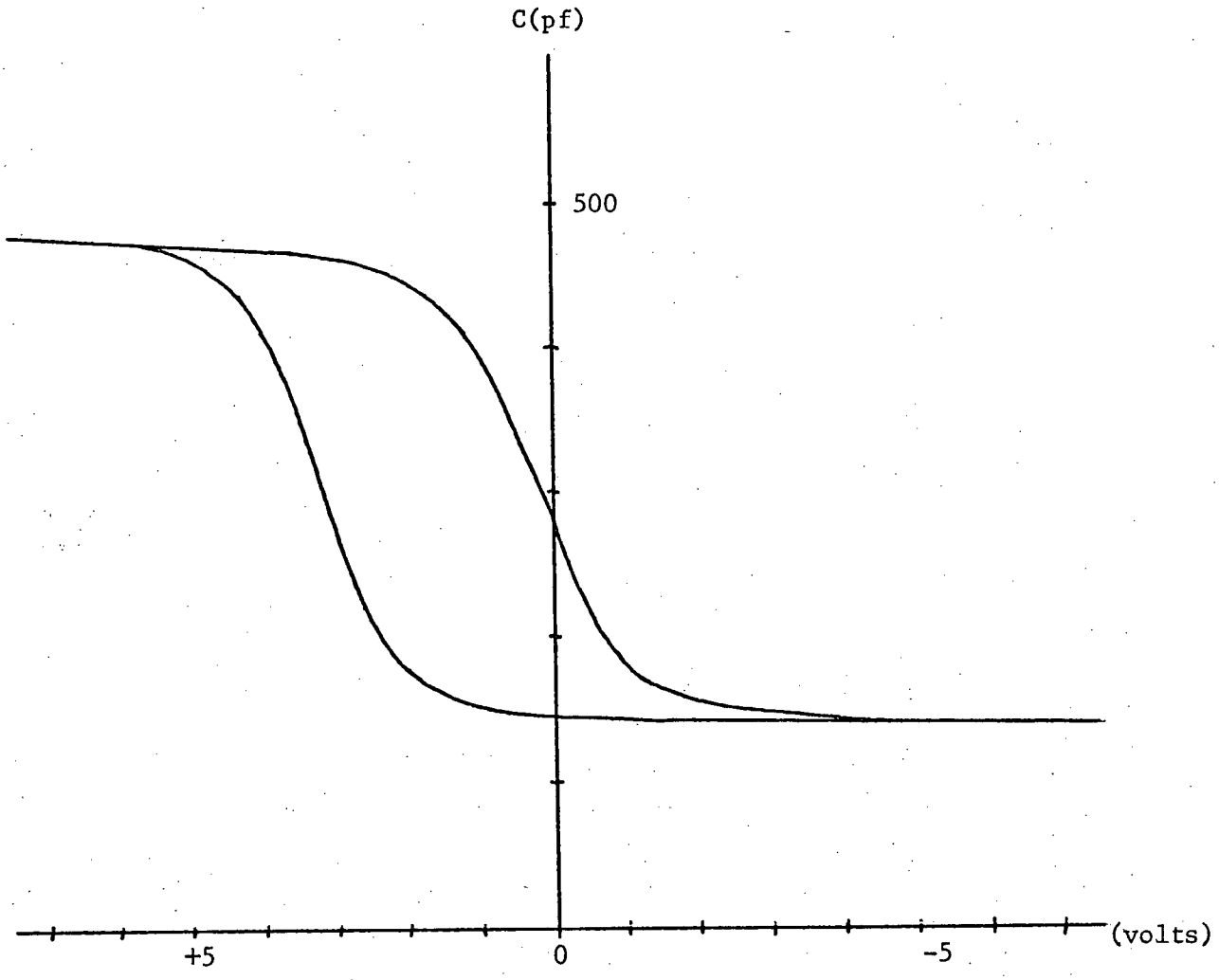

Fig. 3

MOS C Hysteresis (f = 0.01 Hz)

REFERENCES

1. Campbell, K.C. Thin Solid Films , 6(1970) pp. 197-202.

2. Marshak, R.E., Fundamental of Transmission Electron Microscopy , Wiley Interscience, p. 179 (1964).

3. American Institute of Physics Handbook, McGraw-Hill (1967) p. 9-4.

4. Staritzky, E., Analytical Chemistry, 28(1956) p. 2023

5. Hass, G., J.B. Ramsey and R. Thun, J. Optical Soc. Am., 2, 49 p. 116 (1959).

6. Berard, M.F., C.D. Wirkus and D.R. Wilder, J. Am. Cer. Soc., 11, Vol. 51, 643 (1968).

7. Simmons, J.G., Handbook of Thin Film Technology, McGraw-Hill Co., 1970, p. 14-3.

8. Miller, A. and A. Daane, J. Inorg. Nucl. Chem., 9, 27 p. 1955-60 (1965).

9. Dresner, J. and F.V. Shalcross, Solid-State Electron , 5, 205 (1962).

10. Frenkel, J., Phys. Rev. 54, 647 (1938).

11. Mead, C.A. Phys. Rev. J., 128 p. 2088 (1962).

12. Hartman, T.E., J.C. Blair and R. Bauer, JAP 37, p. 2468 (1968).

13. Simmons, J.G. Phys. Rev. 3, 155 (1967).

14. Stuart, M., Phys. Stat. Solidi, 23, 595 (1967).

15. Hill, A.G., A.M. Phahle and J.H. Calderwood, Thin Solid Films 5(1970), p. 278-95.

16. Archer, R.J. "Determination of the Properties of Films on Silicon by the Method of Ellipsometry", J. Optical Soc. Am., Vol. 52, No. 9, pp. 970-977, Sept. 1962.

17. Tallan, N.M. and R.W. Vest, J. Amer. Cer Soc. 8, 49, p. 401 (1966).

18. Fröhlich, H., Theory of Dielectrics, Oxford University Press, London, 1949.

19. Baird, M.E., Reviews of Modern Physics, 1, 40, p. 219 (1968).

20. Cole, K.S. and R.H. Cole, J. Chem Phys. 10, 98 (1942).

21. Fowler, R.H., Statistical Mechanics, Cambridge University Press, 1936 p. 358.

22. Mitchell, K., Proc. Royal Soc. Am., Vol. 146 p. 442 (1924).

23. Schuermeyer, F., J. Appl. Phys. 37 (5) p. 1998 (1966).

24. Goodman, A.M., Electrochem. Soc., Vol. 15 No. 9 p. 276C (1968).

25. Schuermeyer, F., JAP 37 No. 5, p. 1998 (1966).

26. Schuermeyer, F., C.K. Young and J.M. Blasingame, JAP 39 No. 3, p. 1971 (1968).

27. Stuart, R. and F. Wooten, Phys. Rev. 156 No. 2, p. 364 (1967).

28. Powell, R.J., JAP, 40 No. 13, p. 5093 (1969).

29. Grove, A.S., Physics and Technology of Semiconductor Devices, John Wiley and Sons, 1967, p. 271.